Energy & Environmental Science

Carbon-Efficient Conversion of Natural Gas and Natural-Gas Condensates to Chemical Products and Intermediate Feedstocks *via* Catalytic Metal–Organic Framework (MOF) Chemistry

Journal:	*Energy & Environmental Science*
Manuscript ID	EE-REV-03-2022-001010.R2
Article Type:	Review Article
Date Submitted by the Author:	08-Jun-2022
Complete List of Authors:	Liu, Jian; Northwestern University, Chemistry; Argonne National Laboratory, Energy System Devision Yang, Ying; Northwestern University Goetjen, Timothy; Northwestern University, Department of Chemistry Hupp, Joseph; Northwestern University, Department of Chemistry

Energy & Environmental Science

Carbon-Efficient Conversion of Natural Gas and Natural-Gas Condensates to Chemical Products and Intermediate Feedstocks *via* Catalytic Metal–Organic Framework (MOF) Chemistry

Received 00th January 20xx,
Accepted 00th January 20xx

DOI: 10.1039/x0xx00000x

Jian Liu,* Ying Yang, Timothy A. Goetjen, and Joseph T. Hupp*

The net-zero carbon emission scenario of stopping hydrocarbon use as fuel is unlikely to end the extraction of fossil hydrocarbons. Remaining will be a sizable need for hydrocarbons as feedstocks for commodity chemicals destined for transformation into polymers, manufacturing-relevant intermediates, and value-added chemicals. Historically, the primary feedstock source has been oil. Over the past dozen years, however, fracking-based extraction of shale-trapped natural gas from known enormous reserves, in North America, has resulted in feedstock sourcing instead from wet shale gas. This shift has transformed the catalytic chemistry of commodity chemical manufacturing. In this review, following a brief discussion of the merits and limitations of crystallographically well-defined metal–organic frameworks (MOFs) as model catalysts and catalyst-supports, we examined their applications for understanding and potentially enabling carbon-economical, catalytic transformation of C_1, C_2, C_3, and C_4 components of natural gas to desirable commodity chemicals, intermediates, or model compounds.

1. Introduction

Early in this century a convolution of technological, political, and economic considerations kicked off, in North America, a tremendous acceleration of the pace of fracking-based extraction of shale-trapped natural gas from known enormous reserves; see **Figure 1**. The scale of the still ongoing extraction was sufficient to shift the United States from being a massive importer to a net exporter of fossil fuels. Furthermore, the extraction accelerated the decommissioning of coal-fired electrical power plants and their replacement by gas-fired plants and renewable sources. It also led to: a) large regional economic dislocations, both positive and negative, in the extraction sector of the U.S. economy, b) a net reduction in the cost of electrical energy and in the cost of gas-based heating, c) more efficient combustion-based production of electrical energy, and consequently, a diminished output of CO_2 per unit of electrical power, and d) an attenuation of other environmental burdens associated with burning coal, including release of heavy metals, oxy-sulfur compounds, and aerosols, and generation of thorium-contaminated fly-ash as a combustion residue.[1] It has been suggested that while combustion of natural gas produces CO_2, its use could prove to be a beneficial transitional step toward net-zero carbon emissions – pending the build-out of renewable energy production capacity and attendant energy storage capabilities, together with economical carbon-capture and -sequestration.

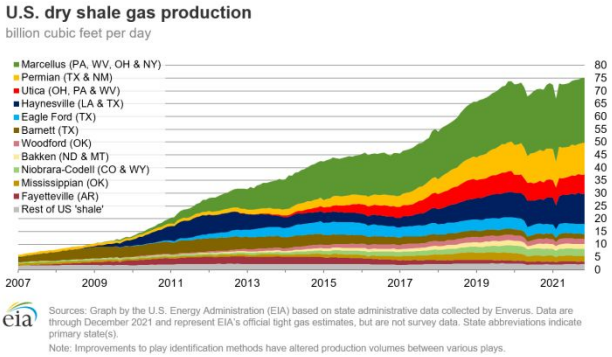

Figure 1. The production of shale gas in the U.S. Source: EIA (2021).

Curiously, a mid-century net-zero carbon emission scenario will not end the extraction of fossil hydrocarbons. Remaining will be a sizable need for hydrocarbons as feedstocks for commodity chemicals destined for transformation into polymers and other value-added chemicals, *i.e.* consumption unrelated to the use of hydrocarbons as fuels. In this realm, the realization of economical extraction of large quantities of natural gas has already resulted, in North America, in extensive replacement of oil by natural gas as a chemical feedstock; see **Figure 2**.[2] Thus, the focus has shifted away from the breakdown of large-hydrocarbon components of crude oil into manufacturing-relevant intermediates, such as naphtha (saturated C_5 to C_{10} mixtures), and toward the build-up of natural gas into manufacturing-relevant intermediates. Notably, shale-derived natural gas, especially from the enormous Marcellus formation, is wet gas – meaning that in addition to methane, it comprises significant fractions of ethane, propane, and butane. Since even ethane, with a critical temperature of 305 K, is liquefiable at room

* *Corresponding authors, Emails: jian.liu@northwestern.edu, j-hupp@northwestern.edu.*
Department of Chemistry, Northwestern University, 2145 Sheridan Rd., Evanston, IL, 60208, United States.
Electronic Supplementary Information (ESI) available: [details of any supplementary information available should be included here]. See DOI: 10.1039/x0xx00000x.

temperature (albeit, only at pressures approaching 50 bar),[3] ethane, propane, and butane are sometimes termed natural-gas liquids, while propane and butane are also termed condensates.

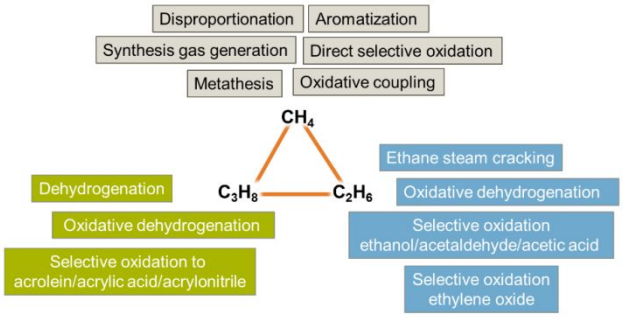

Figure 2. Potential approaches to converting methane and light alkanes, the major component of natural gas, into other valuable products. CH_4 = methane, C_2H_6 = ethane, and C_3H_8 = propane. Adapted with permission from Ref. 2. Copyright 2016 National Academies Press.

The shift from oil to natural gas has transformed the chemistry, and especially the catalytic chemistry, of commodity chemical manufacturing. To oversimplify, the breakdown of crude oil starts with energy-intensive separations, typically distillations, and is followed by high-temperature cracking that converts the heaviest and longest components into lighter hydrocarbons. The common catalysts are zeolites or other alumino-silicates.[4] The harsh conditions for cracking more-or-less guarantee that: a) catalysts will be "nonuniform" (catalyst evolution or aggregation), b) catalyst active-sites will be difficult to identify and characterize with atomic-scale precision, and c) catalyst structures will evolve both with time-on-stream and with regeneration. In contrast, the conditions associated with build-up of useful intermediates from C_1, C_2, C_3, and C_4 hydrocarbons typically are much less harsh, the reactive mixtures are less complex, and the required thermal energy input is less.[5] These are conditions that hold out the possibility of full characterization of catalysts; *operando* observation of catalyst interactions with reactants, intermediates, and products; and *operando* observation and subsequent mechanistic understanding of the chemical and structural evolution of catalysts. More realistically, they hold out these promises for functional model systems that have sufficient stability for such investigations, even if they lack the stability needed for extended, practical utilization. To the extent that these promises are realizable, they may enhance hypothesis-driven design and understanding of heterogeneous catalysts at the atomic or near-atomic scale. In turn or in parallel they can empower both the explanative and predictive capabilities of contemporary computational chemistry. Obviously, the application of computational chemical tools to experimental heterogeneous catalysis becomes much more useful when catalysts are compositionally and structurally uniform, when the compositions and structures are known, when their evolution over time can be accurately followed, and when the corresponding catalyst-synthesis chemistry is well enough developed for desired new or modified catalysts and supports to be realizable experimentally.[6]

In this review, we examine crystallographically well-defined metal–organic frameworks (MOFs) as model heterogeneous catalysts and supports for understanding and enabling chemical transformations of natural gas and natural-gas liquids to relevant or potentially relevant commodity-chemical intermediates and/or products. MOFs are by no means the only materials that hold promise. Others include well-characterized and stabilized catalysts in zeolites;[7] single-atom alloys;[8, 9] single-metal-atom catalysts on high-area, nitrogen-enriched graphite and other supports;[10, 11] and systematically heterogenized, molecular homogeneous catalysts.[12, 13] Our focus is on "carbon-efficient" reactions, and "carbon-efficient" here means no carbon loss as CO_2 and carbon being used to build valuable products in reactions. Following a brief discussion of the merits and limitations of MOFs as model catalysts and catalyst-supports, the review is organized around their application, or potential application, to carbon-economical catalytic transformation of C_1, C_2, C_3, and C_4 components of natural gas to desirable commodity chemicals, intermediates, or model compounds; see

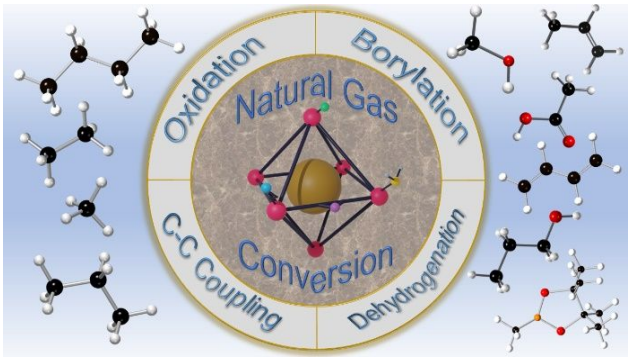

Figure 3.

Figure 3. Catalytic transformation of C_1, C_2, C_3, and C_4 components of natural gas to desirable commodity chemicals or intermediates using MOF-supported catalysts.

2. Discussion

2.1 MOFs as Catalysts and Catalyst Supports

MOFs are typically, but not always, crystallographically well-defined, and microporous, mesoporous, or both.[14] At a minimum, they comprise multitopic organic linkers and metal-containing inorganic nodes, inter-connected in alternating fashion by coordination bonds. Nodes can consist of single metal ions, pairs of metal ions, linker-isolated metal-ion-containing clusters, or shared-linker-terminus-connected one-dimensional rods; see **Figure 4**. Periodically arranged linkers and nodes can yield uniform arrays of pores that are interconnected at the pore-to-pore level by apertures that are similarly uniform. Relevant to heterogeneous catalysis, pores and apertures are often of molecular width. Pores can take the form of distinct cages; channels extending in 1, 2, or 3 directions; pillaring-linker-defined spaces between two-dimensional sheets; or other constructs, see **Figure 4**. Much like zeolites, the various kinds of arrangements are typically defined in terms of approximate network topologies.[15-17] An important subset of MOFs comprises frameworks having topologies equivalent to known zeolite topologies – for example the **sod** or sodalite topology. The members of the subset have been termed Z-MOFs and/or, if they feature imidazole-derived linkers, ZIFs, signifying **z**eolitic **i**midazolate **f**rameworks.[18-20] In contrast to zeolites, however, organic-linker-defined pore and channel walls are typically only one-atom thick.

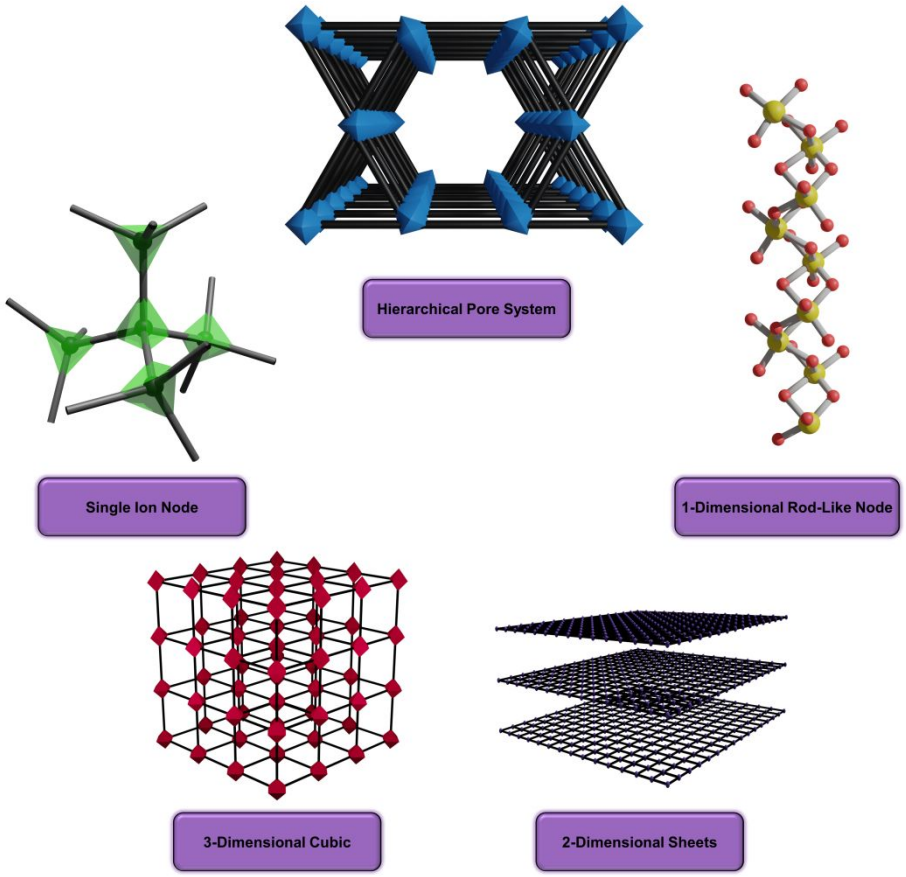

Figure 4. Representative MOF and MOF-component archetypes: ZIF-type single-atom-node architectures, 1D channel with rod-like structures, 2D layered dimensions, 3D cubic structures with high porosity and metal-cluster nodes, and hierarchical porous topologies.

Furthermore, channel walls in MOFs, in contrast to zeolites, tend to be perforated in periodic fashion with small apertures (or even pores) whose presence can escape delineation by approximate topologies and/or experimental pore-size distribution assessments *via* N_2 or Ar isotherm measurements. A common example is the so-called *c*-pore present in most MOFs featuring **csq** topology.[21-24] Experimentally obtained framework topologies typically correspond to kinetic products. In consequence, slight changes in synthesis conditions, synthesis protocols, metal-ion sources, modulator identities and concentrations, and other variables can yield crystallographic distinct, and often strikingly different, polymorphs and topologies.[25-31] An extraordinary example is the family of MOFs having the empirical formula $Zn^{II}(imidazolate)_2$; at least seventeen distinct polymorphs have been synthesized, isolated, and structurally characterized.[32]

MOFs sometimes also include non-structural ligands, such as reactive aqua or hydroxo ligands, post-synthetically displaceable or removable solvent molecules, or similarly displaceable synthesis modulators, *i.e.* monotopic ligands that can slow or otherwise regulate the growth of MOF crystallites.[33-36] The features being regulated can include crystallite morphology, crystallite attachment to a secondary support, defect density, phase purity, and phase or polymorph identity. Defects are distinct from phase impurities. Under-coordinated nodes and/or under-coordinating linkers necessarily exist on the exterior surface of an isolated crystallite and these can behave chemically as if they are structural defects. For crystallites having dimensions of a few tens of nanometers (an ideal size, if the crystallite is used as a drug or enzyme delivery vehicle that would eventually need to pass through human kidneys),[37] the fraction of nodes or linkers residing at the crystallite perimeter can be 0.1 or greater. The most common *true* structural defects are missing linkers and missing nodes, see **Figure 5**.[38-41] Missing-linker defects can enhance diffusive transport of guest molecules, boost gravimetric surface area, and/or expose nodes to reactant molecules.[42] Defect-based node exposure is often essential for engendering MOF catalytic reactivity, and controlled engineering of defect density, location, and identity is important enough to have developed into its own small sub-discipline of MOF chemistry.[43]

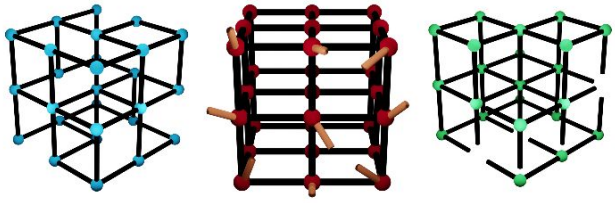

Figure 5. Representative MOF defects: missing linkers (left), discontinuous terminus (middle), and missing nodes (right).

Tens of thousands of MOFs have been described experimentally, with a couple orders of magnitude more having been virtually screened computationally.[44, 45] Roughly five thousand experimental examples have been curated and then described in terms that facilitate their computational or experimental evaluation regarding pore volume, pore size, gravimetric or volumetric surface-area, density, node accessibility, pore-connectivity, approximate topology, and so on.[46] While many are potentially suitable for broad application in heterogenous catalysis,[47] the majority are not. Obviously, the suitability of a particular MOF for heterogeneous catalysis is reaction-specific. To generalize, however, useful MOFs for heterogeneous catalysis will offer: a) molecular-scale porosity,[48] b) good chemical stability toward exposure to H_2, O_2, H_2S, H_2SO_4, HX, NH_3, H_2O_2, N_2O, hydroxide, steam, and/or condensed water,[49] c) good thermal stability,[43] d) good mechanical stability, including stability toward solvent evacuation and associated capillary forces,[50] e) overall crystallinity, and f) uniformity of active-site composition and structure, even at the scale of single atoms.

Good to excellent thermal stability for MOFs translates as sustained retention of framework crystallinity and porosity (days or weeks) at 350 or 400 °C, although: a) nonstructural, charge-neutral ligands such as H_2O are typically lost at much lower temperatures, and b) MOFs characterized by comparatively weak node-linker bonds can lose crystallinity and even structural integrity at much lower temperatures, *e.g.* 200 °C or below.[51-54] Above 450 or 500 °C in air, even the most robust MOFs tend to fragment and/or combust. Under static N_2 or N_2/NH_3 atmosphere, at temperatures around 550 °C or higher, MOFs pyrolyze to yield new materials resembling high-surface-area graphite, often with metal atoms from MOF nodes embedded as reactant-accessible, single-metal-ions that are competent for heterogeneous catalysis or electrocatalysis.[55-57] These interesting materials are outside the scope of the review. Returning to the issue of thermal stability, we can conclude that MOFs are best viewed as complementary to zeolites, high-surface-area metal-oxide powders, and related materials, as catalysts or catalyst supports, as MOFs are ill-suited for reactions at temperatures more than a few hundred degrees above room temperature. Nevertheless, it is remarkable that frameworks consisting largely of hydrocarbon linkers can be usefully deployed as catalysts or catalyst supports for substrate oxidation by O_2 at a few hundred degrees Celsius without being lost to combustion. MOF-catalysed oxidative dehydrogenation of propane to propene at 230 °C[58] and cyclohexene to benzene at 350 °C[59] are two such examples.

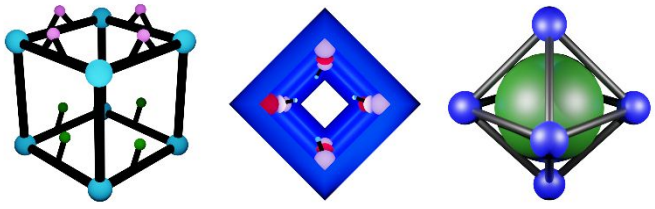

Figure 6. Representation of modes of use of MOFs as catalysts or catalyst-supports, including linker-supported catalysts (left), nodes as catalysts or node-supported catalysts (middle), and MOF encapsulated or enshrouded nanoparticles (right).

As shown qualitatively in **Figure 6**, depending on the identity of the MOF, active-sites for heterogeneous catalysis can consist of functionalized linkers, coordinatively unsaturated metal ions on nodes, enshrouded nanoparticles, noncovalently linker-adhering polyoxometalates, non-structural ligands such as metal complexes intentionally grafted after framework synthesis, or node-grafted metal ions, metal-oxy clusters, metal-sulfide clusters, or other species.[60-69] Thus, the MOF itself can be viewed as either a catalyst or a catalyst support. Relevant to catalytic C_1, C_2, C_3, and C_4 chemistry, commonly encountered support-like nodes are hexa-zirconium(IV) species having a core structure of $Zr_6(\mu_3\text{-}O)_4(\mu_3\text{-}OH)_4$. The node can accommodate up to twelve linker-terminating carboxylate groups, and MOFs are known with 4-connected,[70] 5-connected,[71] 6-connected,[25] 8-connected,[72] 9-connected,[73, 74] and 10-connected nodes,[75, 76] in addition to nominally 12-connected nodes.[30] Connection sites not occupied by linker carboxylates are typically occupied by non-structural ligands and/or terminal aqua/hydroxo pairs.[25, 34, 77] These ligands, together with bridging hydroxo ligands are ideal for grafting metal-ions or clusters. If these ligands are displaced by candidate reactants or removed thermally, the underlying metal(IV) sites can function as Lewis acids,[51, 78, 79] or, in the case of displacement by sulfate, nodes can be made highly Brønsted-acidic[80-82] – indeed, nearly super-acidic, *i.e.* nearly as acidic as concentrated sulfuric acid[71]— where the most widely studied example is sulfated MOF-808 (Zr.QMKYBPDZANOJGF.MOFkey-v1.spn).[25]

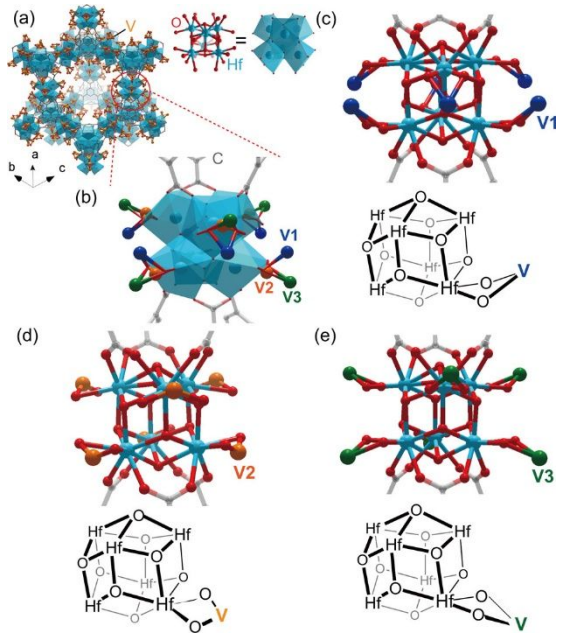

Figure 7. An example of SCXRD observation of catalyst evolution. After heating Hf-MOF-808-V overnight at 105 °C, the catalyst evolves from a version featuring three crystallographically distinct single-V-atom sites (V1, V2, and V3) to a version with only one type of single-V-atom site (V2). Adapted with permission from Ref. 96. Copyright 2018 American Chemical Society.

Thus, nodes within MOFs of this kind can be viewed as tiny pieces of zirconia or other metal-oxides having well-defined and uniform composition.[83] In many cases the uniformity translates into

atomically precise single-crystal X-ray diffraction (SCXRD) structures featuring subsequently grafted catalytic ions and clusters.[62, 67, 81, 84-95] In a few cases, SCXRD measurements reveal how a grafted catalyst evolves over the course of catalytic runs, or changes in response to catalytically relevant thermal or chemical pre-treatment; see **Figure 7**.[94, 96] Analogous core structures and support behaviour have been described for hafnia-, ceria-, and thoria-like fragments/nodes[62, 86, 97, 98] and for nodes featuring twelve rather than six M(IV) ions.[99, 100] For less oxophilic metals in lower oxidation states, stable frameworks can often be obtained by enlisting anionic nitrogen ligands, such as di-, tri-, or tetra-azolates, as linkers.[101, 102]

A mechanistically useful feature of linker-isolated nodes is their propensity to block node-to-node migration and sintering of grafted ionic catalysts – for example, metal ions or metal-ion-containing clusters.[76, 90, 92, 103-106] This behaviour contrasts with the typical behaviour of metal-oxide powders as supports; the absence of migration and sintering is potentially quite powerful for answering questions relating to the effects of metal-nuclearity in defining catalytic activity and selectivity, and for distinguishing between mechanisms for catalysed reactions.[107, 108]

While less significant for MOF-based catalytic chemical transformations of natural gas than for many other kinds of chemical transformations, it is worth mentioning that MOF linkers can be enlisted for ligation and presentation of non-structural catalytic metal centres.[109-111] Linkers can also be used for presentation of catalytic or co-catalytic acids, bases, or their conjugates[112] – for example, in the form of substituent amines, imines, carboxylates, or sulfonates.[113]

Like many zeolites and related materials (MCM-41, SBA-15, etc.), names for MOFs are typically assigned by the groups who first report them and often acknowledge institutions where the labs are located (*e.g.*, UiO signifies University of Oslo). Schemes for further designation differ from lab to lab and with some MOFs having multiple common names (*e.g.*, MOF-74 vs. CPO-27). Bucior *et al*.[114] recently developed two systematic MOF identifiers, MOFid and MOFkey, by deconstructing MOFs into their building blocks and underlying topological networks. Applying their algorithms, we have assigned each MOF in the review a unique MOFid and MOFkey; see **Table 1**.

2.2 Conversion of C_1 Hydrocarbons

Oil extraction *via* fracking technology is typically accompanied by unwanted extraction of natural gas. In the absence of gas-dedicated pipelines, it is cheaper to flare natural gas to CO_2 and water vapor than to capture the gas and ship it – for example, by rail, as is done with oil when pipeline capacity is insufficient. Methane is the main component of natural gas, including wet shale gas. Most of the extracted methane is burned for heating, including heating to power steam turbines for electricity generation. Combustion yields CO_2, most of which is released into the atmosphere. By far the largest non-combustion use for methane is H_2 formation *via* steam reforming (**eq. 1**) followed by the water-gas shift reaction and necessary, but undesirable, CO_2 formation (**eq. 2**):

$$CH_4 + H_2O \rightarrow CO + 3\,H_2 \qquad (1)$$

$$CO + H_2O \rightarrow CO_2 + H_2 \qquad (2)$$

The largest uses for methane-derived H_2 are for Haber-Bosch based ammonia synthesis, chiefly for fertilizer, and for hydrocracking petroleum. In principle, these uses could be displaced by H_2 production at scale *via* electrolysis of water, either photoelectrochemically or *via* photovoltaic-supplied electrical energy in combination with electrocatalysts. An attractive, but not yet feasible, alternative to flaring would be to catalytically transform methane gas to methanol liquid,[115, 116] inexpensively, at the well-head, using easy-to-relocate equipment that is practical to employ on a much smaller scale than required for economical production of methanol from syn-gas ($CO + H_2$).

Methanol is used for production of formaldehyde, a high-volume commodity chemical intermediate. It is also used for synthesis of olefins, most notably ethylene and propylene – the two highest volume chemicals for polymer synthesis. The carbon-efficient, methanol-to-olefin (MTO) process entails dehydration of methanol, most likely initially to dimethylether (DME), followed by further dehydration and formation of hydrocarbon mixtures within large pores of silicoaluminophosphate-34 (SAPO-34),[117] Zeolite Socony Mobil-5 (ZSM-5), or other zeolite-based catalysts, with ethylene or propylene then selectively exiting through small pores;[118-120] see **eq. 3**. Larger species in the hydrocarbon pool, including five- and six-carbon chains continue interconverting, with newly formed ethylene and propylene continuously exiting the pool in size- and shape-selective fashion. Key to zeolite catalytic activity is the ability of Al(III)-connected, bridging O-H sites in the zeolites to function as Brønsted acids.[121] These acids can react with methanol to yield H_2O and to adsorb or bridge methoxide, from which CH_3^+ can be supplied to other species, thereby enriching the composition of the hydrocarbon pool.

$$2CH_3OH \xrightarrow{H_2O} CH_3OCH_3 \xrightarrow{H_2O} CH_2CH_2 \qquad (3)$$

2.2.1 MTO-relevant Catalysis by MOFs.

The MTO process, while designed to run at ~ 470 °C, can operate at temperatures as low as 300 °C,[122] – albeit sub-optimally, as coking is extensive and rates are slow. This temperature is within the thermal stability of many MOFs, but not all. Hierarchically porous, size- and shape-selective MOFs exist, as do MOFs featuring large cavities linked by small apertures, *i.e.* geometries that could be compatible with the hydrocarbon pool concept, but none has been reported for MTO. The most persuasive MOF-based example of hydrocarbon-pool type behaviour is probably Ahn's study[123] of the selective catalytic isomerization of xylene mixtures by cages bounded by zirconia-like MOF nodes together with polyoxometalates that are size-matched to MOF micropores in a hierarchically porous MOF, NU-1000 (Zr.HVCDAMXLLUJLQZ.MOFkey-v1.csq). Nevertheless, the interaction of alcohols with Brønsted acids, the formation of adsorbed/grafted alkoxides, catalytic dehydration of methanol to DME, ethanol to diethylether and ethylene, and *t*-butanol to isobutene have been studied in some detail.[124, 125] These studies, chiefly by Gates and co-workers,[126] have been with MOFs that present well-defined Al(III)- or Zr(IV)-oxy, hydroxy species (rods (Al)

or clusters (Zr)) as nodes,[126-129] *e.g.* MIL-53(Al),[130] MIL-68(Al),[131] UiO-66,[30] hcp-UiO-66,[132] NU-1000,[24] Al-AIM-NU-1000,[133] and MOF-808;[25] see **Figure 8**.

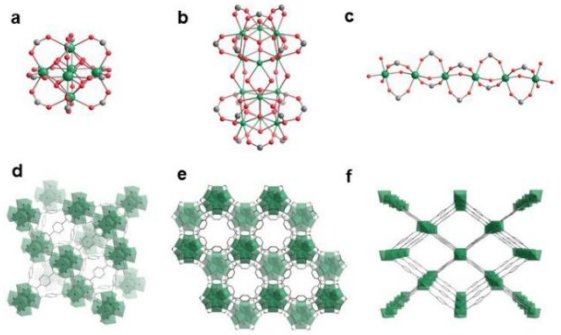

Figure 8. (a) Zr_6 node structure in UiO-66, NU-1000, and MOF-808; (b) $Zr_{12}O_{22}$ node in **hcp** UiO-66; (c) $[Al(OH)]_n$ node in MIL-53 and MIL-68; MOF structures of (d) UiO-66, (e) hcp UiO-66; (f) MIL-53. Color code: red, oxygen; green, zirconium or aluminum; grey, carbon. Adapted with permission from Ref. 126. Copyright 2021 American Chemical Society.

2.2.2 Selective Partial Oxidation to Methanol

2.2.2.1 Using O_2 as Oxidant

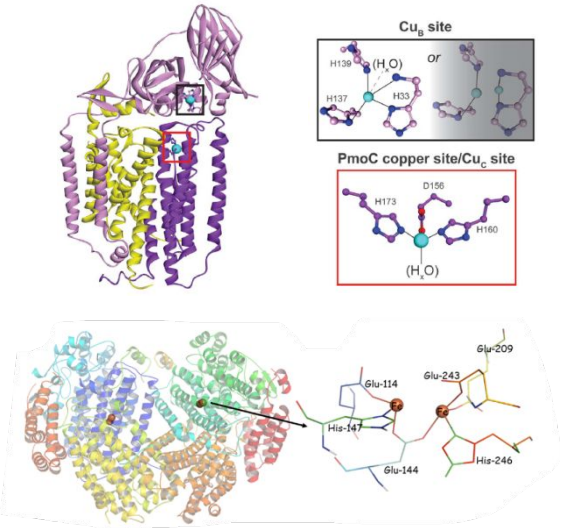

Figure 9. Structure of copper-based particulate MMO (pMMO) and its mononuclear copper centres (top) and iron-based soluble MMO (sMMO) and the dinuclear iron centre (bottom). Adapted with permission from Refs. 141 and 142. Copyright 2017 American Chemical Society and 2019 Science.

Desirable, but little practiced abiotically, is selective partial oxidation of methane to methanol with O_2 as the oxidant;[134-137] see **eq. 4**.

$$CH_4 + 0.5\ O_2 \rightarrow CH_3OH \qquad (4)$$

This reaction is catalytically challenging because: a) the strong C-H bonds of methane are intrinsically inert, b) reactions of ground-state (triplet) dioxygen with singlet reactants are spin-forbidden, c) the initial oxidation reaction is appreciably exothermic, thus, can facilitate activation of subsequent steps, and d) the barriers to further oxidation to formaldehyde, CO, and CO_2, are typically smaller than the barrier for conversion of methane to methanol. Consequently, reaction of methane with O_2 is often plagued by oxidation to products beyond methanol. Nevertheless, copper- and iron-based methane monooxygenases (MMO enzymes in **Figure 9**)[138-142] are known to execute the partial oxidation rapidly, selectively, and at ambient temperature. An obvious strategy for abiotic selective partial oxidation of methane would be to emulate the active-sites of MMOs by incorporating artificial constructs within MOF pores. The frameworks would ideally then prevent active-site sintering or agglomeration, while permitting reactant ingress and product egress. In its most sophisticated form, the MOF-isolation approach could include independent positioning of chemically appropriate protein-residue-like moieties proximal to active-sites.

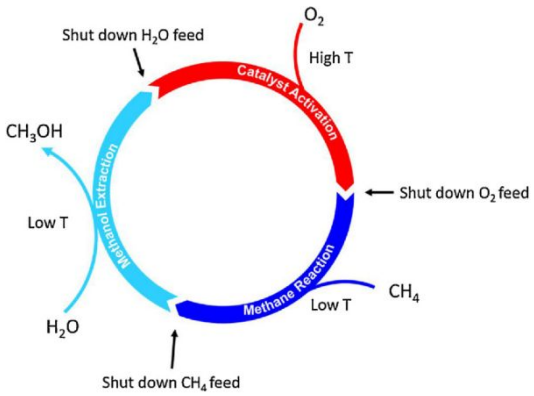

Figure 10. Schematic illustration of chemical looping for selective methane oxidation to methanol. Adapted with permission from Ref. 148. Copyright 2018 Elsevier.

C-H attack clearly is an important early step in catalysing the conversion of methane to methanol; however, recent studies with copper-catalyst-containing zeolites,[143-145] and subsequently MOFs,[146-148] have shown that reaction progress in abiotic systems may be arrested by tenacious adsorption of product methanol, making product desorption a rate-limiting step. While strong methanol binding can slow or altogether stop catalyst turnover, it can also serve to inhibit over-oxidation. Reactions can be advanced, however, by turning to chemical looping.[149] For methane oxidation, the process can be separated into sequences involving: 1) active-site exposure to an oxidant to generate a potent oxyl species, 2) dosing with the alkane, C-H attack by metal-oxyl species, and trapping of the product, for example as a methoxide bridged between two metal ions, and 3) oxidant-free desorption and collection of methanol under forcing conditions, such as prolonged exposure to steam – desorption being difficult because two metal-oxygen bonds must be broken. Spatial and temporal separation of free methanol and the oxidant prevents over-oxidation. In principle, one full loop is the equivalent of one catalytic turnover; see **Figure 10**. As an aside, an alternative to oxo-bridged dicopper active-sites that lead to methoxide- or methanol-bridged dicopper intermediates (*i.e.* bridging species that are difficult to dislodge and recover as free methanol) would be terminal-oxo metal sites as catalysts. A methane-derived methanol or methoxide intermediate would then need to break only one metal-oxygen bond, rather than two, to escape as a recoverable product molecule and reset the catalyst for oxidant binding and a second cycle of C-H bond activation. Unfortunately, beyond group 8, transition metals in tetragonal

coordination environments do not form isolable terminal-oxo complexes – an observation termed by Winkler and Gray the "oxo wall"[150, 151] and readily understandable from ligand-field theory. Recall that copper is a group 11 element.

The first successful demonstration of looping-like, partial oxidation of methane by a MOF-supported catalyst was reported by Ikuno and co-workers.[147] Copper-oxo clusters were incorporated within a Zr-based MOF, NU-1000, *via* an automated ALD-like (ALD = atomic layer deposition) sequence involving the reaction of vapor-phase bis-(dimethylamino-2-propoxy)copper(II) with node-sited O-H groups, followed by treatment with steam to remove unreacted dimethylamino-2-propoxide from the installed copper ions. *In situ* X-ray absorption near-edge structure (XANES) spectroscopy measurements showed that 9% of the installed Cu(II) was reduced to Cu(I) during and following methane loading. Combined extended X-ray absorption fine structure (EXAFS) spectroscopy and density-functional theory (DFT) studies indicated that the dominant form of copper is a linear, trimeric Cu-hydroxide-like cluster bridging two Zr_6 nodes and spanning the *c*-pore of NU-1000 (**Figure 11**). This material exhibited 60% methanol selectivity (with dimethyl ether included) in a plug flow reactor under 150 °C and atmospheric pressure, albeit with a low yield for methanol + dimethylether (13.3 μmol/g_{cat}; 0.03 mol/mol_{Cu}), see **Table 2**.

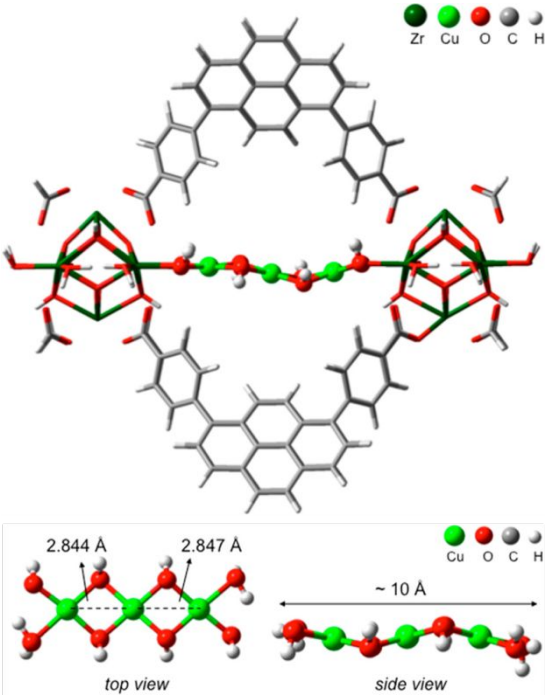

Figure 11. (Top) DFT-optimized structure of trimeric $Cu(OH)_2$ located between two nodes of MOF NU-1000; and (Bottom) ~ 10 Å trimer from top and side views. Adapted with permission from Ref. 147. Copyright 2017 American Chemical Society.

Computations indicate that key to reactivity is substantial oxyl character for a bridging hydroxo ligand that inserts into a C-H bond of methane to yield a bridging methanol or methoxide, *i.e.* a species bound to two copper ions.[147] This configuration would account for the need for forcing conditions – prolonged exposure to O_2-free steam – to release the formed methanol. The nearly complete absence of over-oxidation is presumably a consequence of the copper-based immobilization of methoxide or methanol, as immobilization would preclude subsequent O_2 binding and activation for conversion of methanol to formaldehyde, formate/formic acid, CO, or CO_2. Only after methanol release and recovery is O_2 added to regenerate the reactive, all Cu(II), trimeric species.

Follow-up work from the same group[146] focused on a closely related material denoted as Cu-SIM-NU-1000. This material was obtained through **s**olvothermal deposition **i**n **M**OFs (SIM) with aqueous copper(II) acetate as the metal precursor. Potentially relevant is that the precursor is present in water mainly as a pair of cupric ions bridged by each of four acetate ions that define a pair of square-planer oxy-anion coordination environments, with one of two axial sites on each copper ion accessible and potentially available for coordination of a fifth ligand. After a careful screening of operation parameters (methane activation time, temperature, pressure, and Cu loading), the single-loop production of methanol (with dimethyl ether included) was improved to 0.04 mol/mol_{Cu} at 200 °C and 40 bar, with a selectivity of ~90% (see **Table 2**). A recycling test verified the stability of Cu-SIM-NU-1000. EXAFS analyses showed that by increasing the Cu loading, the dominant speciation can be shifted from single copper ions to dimeric, oxo-bridged, Cu(II). The results of DFT calculations support the stability of the dimeric structure and suggest that the high selectivity for methanol arises from C-H attack by some form of the prevalent dicopper oxyl units (see **Figure 12**). The combined findings suggest that avoiding product trapping may be one reason why the active-site of pMMO evolved with monomeric copper.

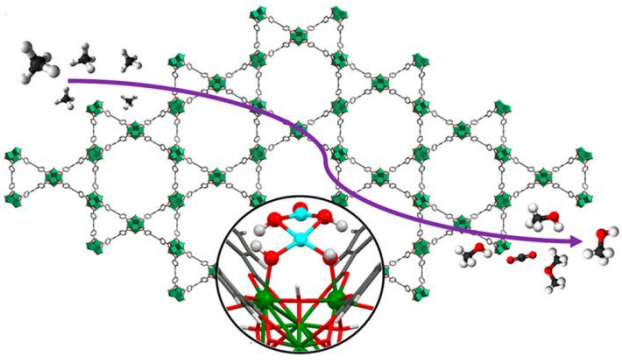

Figure 12. DFT-optimized structure of dinuclear complex $[Cu^{II}_2(OH)_4(H_2O)]$ on the MOF node in Cu-SIM-NU-1000. Adapted with permission from Ref. 146. Copyright 2019 American Chemical Society.

Note that in both studies involving NU-1000 as a support, less than 10% of the installed copper ions are functional for methane oxidation. Thus, despite the promise, or at least potential, for site uniformity offered by crystallographically characterized frameworks, structurally undetected, minority forms of few-copper-atom units appear to be responsible for selective partial oxidation of methane to methanol. The majority dimeric or trimeric hydroxo- or oxo-bridged copper species, as identified by a battery of structural tools (albeit, not single-crystal X-ray crystallography), are evidently neither ideally reactive nor overly reactive toward methane, but simply *un*reactive.

Very recently, Ren *et al.* reported qualitatively similar chemical-looping based methane oxidation to methanol, and a trace of

ethanol, *via* O_2 with oxy-Cu(II) clusters sited in the pores of a derivative of UiO-67.[152]

2.2.2.2 Using H_2O_2 as Oxidant

The sole experimental example of MOF-catalyst-facilitated, continuous selective partial oxidation of methane is from Gascon and co-workers[153, 154] and relies upon a mixed-metal MOF, MIL-53(Al, Fe) (Al: Al.KKEYFWRCBNTPAC.MOFkey-v1.rna, Fe: Fe.KKEYFWRCBNTPAC.MOFkey-v1.rna). This material, which was electrochemically synthesized, features chains rather than clusters as nodes (see **Figure 13**), and employs the MOF itself, rather than a grafted entity, as the catalyst. Characterization by electron paramagnetic resonance (EPR) and Mössbauer spectroscopy pointed to the presence of both mononuclear and dinuclear iron species within the octahedral [AlO_6] chain, *i.e.* sites at least nominally resembling the iron-containing active sites in sMMO.[141, 153] The employed oxidant, H_2O_2, is unlikely to be economically practical for manufacturing, but H_2O_2 is much easier to activate than O_2 and it is a two-electron, rather than four-electron, oxidant. Batch reactor studies in aqueous H_2O_2 revealed catalytic conversion of methane to methanol, methyl peroxide, formic acid, and CO_2 with a maximum turnover frequency (TOF) close to 90 h^{-1} and selectivity for oxygenates of 80% (see **Table 2**). DFT studies suggested that both iron species can catalyse methane oxidation, but indicated for dimeric iron a lower energy barrier for rate-limiting C-H activation. Figure 13b presents a possible mechanism. As shown in step 2, reversible partial dissociation of a linker-terminating carboxylate group from iron, concomitant with hydrogen peroxide binding to iron, is thought to be key to activation of the oxidant. Thus, homolytic dissociation of iron-bound H_2O_2 is facilitated by a bridging hydroxo ligand; again see scheme proposed in Figure 13. Notably, pure MIL-53(Fe) is unstable in water, and therefore of limited value despite the high density of potential catalytic sites. The MOF can be rendered water-stable, however, by replacing the majority of the material's Fe(III) ions by redox-inert and substitutionally inert Al(III).

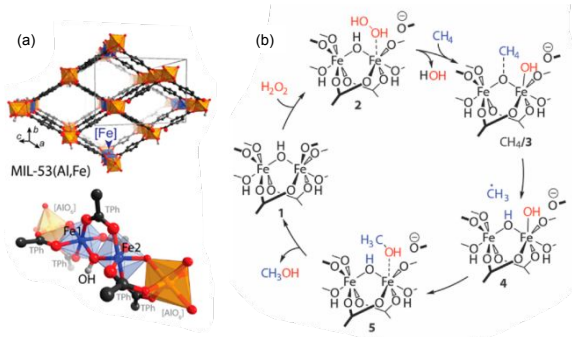

Figure 13. (a) Site-isolated Fe ions in the MIL-53 octahedral [AlO_6] chain; (b) Proposed reaction mechanism on diiron sites in MIL-53(Al, Fe) for methane oxidation with H_2O_2. Adapted with permission from Ref. 153. Copyright 2018 American Chemical Society.

2.2.2.3 Using N_2O as Oxidant

N_2O is usually viewed as too expensive for use in high-volume chemical manufacturing. Nevertheless, it is clearly useful for mechanistic studies. In contrast to triplet O_2 (ground-state O_2), its reactivity toward singlet co-reactants, *e.g.* most organic chemicals, including those comprising natural gas, is not inhibited by spin restrictions. Additionally, it disposes of the common oxidative catalysis problem of what to do with the second oxygen atom of O_2. With a nitrogen-oxygen bond-dissociation energy of ~ 167 kJ/mol, its use as an oxidant typically requires elevated temperatures or catalytic activation.

Copper active-sites in pMMO are ligated by histidine residues (imidazole-containing residues). Baek and co-workers reported a series of pMMO-inspired MOF-supported dicopper species for selective partial oxidation of methane.[155] A zirconium-based MOF, MOF-808, was post-synthetically node-modified with various imidazole- or benzimidazole-presenting ligands, capable of binding Cu(I) and ultimately yielding bis(*μ*-oxo) dicopper species; see **Figure 14**. To note, when this work was done, the prevailing view was still that the active-site of pMMO is dinuclear in copper, rather than mononuclear.[142, 156] Following activation (oxidation) by N_2O, in a scheme probably best-described as chemical looping, the copper-modified frameworks indeed did facilitate oxidation of methane to methanol, with 100% selectivity at 150 °C. The observed turnover number (TON), however, was only ~ 0.02 mol/mol_{Cu} (**Table 2**), with the materials displaying diminished TONs in subsequent cycles. As the experiments were run at a methane pressure of only 1 bar, it is conceivable that only a tiny fraction of reactive copper-oxyl species encounter CH_4. Alternatively, it may be that only a tiny sub-population of copper-oxyl sites are intrinsically active. As an aside, pre-treatment of these materials by heating under an inert (helium) atmosphere at 150 °C for 1 hour is accompanied by auto-reduction of a fraction of Cu(II) to Cu(I) ions – an unexpected finding. In its as-prepared form, MOF-808 features formate ligands, in place of anticipated aqua and hydroxo ligands.[25] Based on recent work by Yang and co-workers (with NU-1000) node-ligated formate can function as a sacrificial two-electron donor, with copper ions as electron acceptors.[94] In both studies (Baek, *et al.* and Yang, *et al.*) the unexpected auto-reduction of copper together with the observed or inferred consumption of non-structural ligands can be viewed as examples of catalyst evolution.

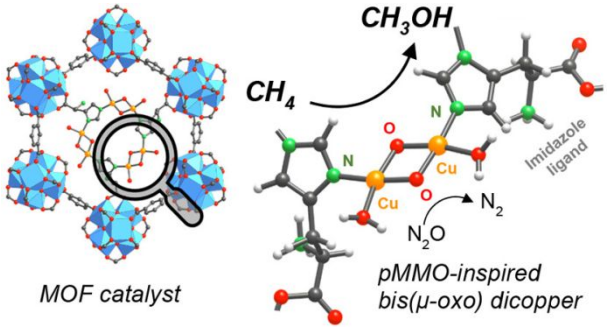

Figure 14. Bis(*μ*-oxo) dicopper sites supported by MOF-808 for methane oxidation. Adapted with permission from Ref. 155. Copyright 2018 American Chemical Society.

One might anticipate that chemical-looping could be avoided and that continuous, catalytic, selective-partial-oxidation of methane could be accomplished by simultaneously feeding to a catalyst-containing flow-reactor the alkane, an oxidant, and product(methanol)-displacing steam. This kind of behaviour has yet to be demonstrated for a MOF-supported copper catalyst. With O_2 as oxidant, it has yet to be demonstrated for any MOF-supported or MOF-based catalyst (although it has been demonstrated with metal

ions in zeolites[143]). Perhaps the recent demonstration/realization that the active-site within particulate methane monooxygenase is characterized by a single copper ion[142] will be the insight that culminates in success with MOF-supported catalysts.

The modular nature of MOF structures is such that even for a small set of MOF building blocks (linkers and nodes, or their chemical precursors), an enormous number of likely synthetically accessible, candidate materials can be identified.[157] Computational screening can serve to narrow the synthesis field and thereby decrease the number of candidates to be targeted experimentally. Computational studies also, of course, can yield mechanistic insights – in some cases by introducing variant compounds that systematically modulate a structural or electronic feature. DFT calculations are typically the computations of choice for mechanism elucidation for MOF-based or MOF-supported catalysts. These computations, in contrast to, say, evaluation of host (MOF)/guest (molecule) interactions *via* standard force fields, are not readily scalable to encompass enormous numbers of candidate materials. However, their strategic use on the scale of, say, dozens of related candidate compounds/catalysts is feasible.[67, 68, 85, 158, 159]

An oxidation-relevant illustration comes from Liao, Getman, and Snurr,[160] and concerns alkane (specifically ethane, rather than methane) C-H activation for formation of alcohols, as catalysed by coordinatively unsaturated metal sites, starting with variants of MOF-74(Fe) (Fe.YXUXCIBWQAOXRL.MOFkey-v1.etb)[161] (also sometimes termed CPO-27(Fe),[162] or simply Fe_2(dobdc)[163] where dobdc is 4,4'-dioxido-3,3'-benzenedicarboxylate and CPO denotes Coordination Polymer of Oslo) and extending to include other MOFs presenting coordinatively unsaturated iron ions. The impetus for the computational study was the observation by Long and co-workers of selective partial oxidation of methane to methanol and ethane to ethanol using N_2O in the presence of Fe-MOF-74[161] – work that is discussed further in the section below, devoted to C_2 chemistry.

In the Liao study, a strong, inverse correlation of the energy for metal-oxo active site formation and for C-H activation was uncovered for open iron sites within MOF-74 and derivatives having linker substituents.[160] This correlation was subsequently found (computationally) by Rosen[164] to extend to 60 MOFs featuring single metal ions across a range of metal identities and coordination environments, provided that there is no change in bond-order between the metal centre and the remaining atoms as a consequence of metal-oxo bond formation (**Figure 15**). In the figure, the computed metal-oxygen bond formation energies are referenced to O_2 as the oxidant, but the correlation itself is agnostic regarding the source of oxygen. Thus, an axis-shifted, but otherwise identical, correlation would be obtained with N_2O as oxidant. By way of comparison, the bond dissociation energies (BDEs) for O_2 and N_2O, respectively, are 498 kJ/mol and 167 kJ/mol. Here the term "single metal ion" means redox participation of one metal ion, even if sited proximal to multiple spectator metal ions. Thus, the entries in **Figure 15** include MOFs having nodes of composition $M^{3+}{}_2M^{2+}(\mu_3\text{-}O)(RCOO)_6$, such as versions of MIL-100, MIL-101, and PCN-250. The trade-off between active-site stability and the barrier for C-H activation implies a predictive design rule for MOF-based catalysts and could be effective for screening and selecting MOFs for subsequent experimental study. In addition, the observed need to conserve bond-order in order to retain the correlation, *i.e.* scaling relationship, suggests that the scaling relationship can be intentionally broken by coupling the formation of the active-site with the reversible formation/cleavage of another bond (*e.g.*, metal-metal bond, metal-ligand bond, or possibly even hydrogen bond).

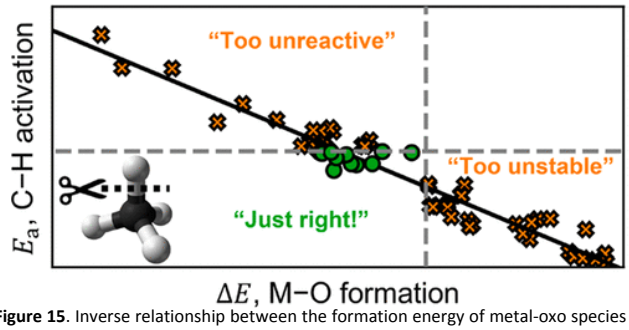

Figure 15. Inverse relationship between the formation energy of metal-oxo species and the activation energy of C-H bond for methane oxidation. Adapted with permission from Ref. 164. Copyright 2019 American Chemical Society.

Barona and Snurr extended the computational study to methane oxidation to methanol with N_2O *via* catalytic MOFs containing mixed-metal compositions and overall trinuclear metal nodes.[165] As illustrated by **Figure 16**, the computations predict broad tunability of both the barrier to N-O bond activation and the barrier to C-H activation.

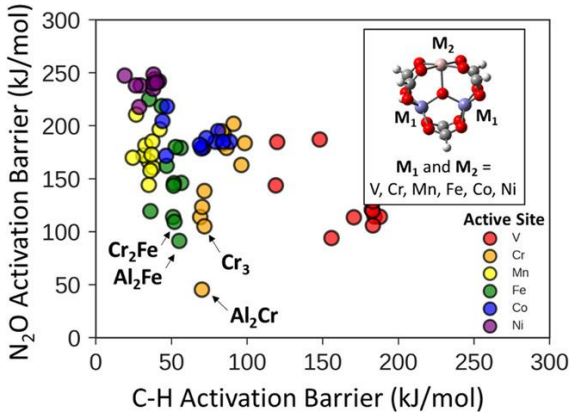

Figure 16. Influence of spectator atoms on the catalytic activity of a specific metal site in the cluster in MOFs toward the N_2O activation and C–H bond activation steps of the partial oxidation of methane to methanol. Adapted with permission from Ref. 165. Copyright 2020 American Chemical Society.

Vitillo and co-workers reported qualitatively similar computational results and examined both methane and ethane as reactants.[166] They showed that weak, second-sphere interactions with either a reactive hydrogen atom from methane or a reactive, node-bound oxygen atom can modulate the energy of the transition-state for C–H bond breaking for derivatives MIL-101(Fe).[167] As suggested in simplified form in **Figure 17**, electron-withdrawing or electron-donating substituents of MOF linkers can be used to introduce the second-sphere interactions. They further observed computationally that the energy for the transition-state for rate-determining N_2 release from node-coordinated N_2O can be

systematically lowered *via* the interaction of the oxygen atom of coordinated N_2O with linker-sited, electron-withdrawing groups.

Figure 17. Noncovalent interactions as hydrogen bond stabilizing the different

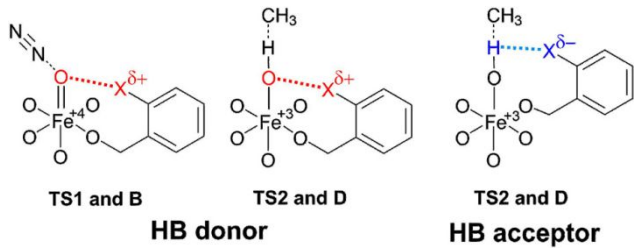

intermediates of the reaction. Adapted with permission from Ref. 167. Copyright 2020 American Chemical Society.

Given that strongly Lewis basic linkers/ligands can stabilize metal-ion-based active-sites, metal–azolate frameworks (MAFs) offering open metal sites ought to be promising for C-H activation.[20] Rosen and co-workers computationally investigated a series of triazolate-based MAFs, M_2X_2(BBTA) (M = metal, X = bridging anion, H_2BBTA = 1H,5H-benzo(1,2-d:4,5-d')bistriazole), encompassing a variety of metals and a variety of bridging anions, as catalysts for alkane oxidation.[168] They found that for early transition metals, bridging ligands with greater basicity can better stabilize $[MO]^{2+}$ moieties, whereas the influence of bridging-ligand basicity is negligible for later ones. In comparison to MOFs having carboxylate-coordinated metals as oxo-forming active-sites, those with azolate-coordinated metal ions were generally predicted to be superior for C-H activation. Detailed spin-density analyses during C-H activation revealed a ferromagnetic to antiferromagnetic transition for Fe- and Mn-based MAFs, which translates to an increase in spin density on the metal centre and a greatly reduced kinetic barrier.

2.2.3 Selective Partial Oxidation and Carbon-Carbon Coupling to Convert Methane to Acetic Acid

Worldwide acetic acid production is on the order of 10 million tonnes per year, with most of the product used for production of chemical intermediates such as vinyl acetate monomer and terephthalic acid. The acid is largely obtained from carbonylation of methanol using $[Ir(CO)_2I_2]^-$ or $[Rh(CO)_2I_2]^-$ as a homogeneous solution catalyst and HI as a co-catalyst.[169]

While not used commercially, acetic acid can also be obtained directly from methane by using much less precious oxy-vanadium(IV) species as homogeneous catalysts, together with $S_2O_8^{2-}$ as oxidant, all in trifluoroacetic acid (TFA).[170, 171] Under these conditions, methane supplies the methyl group, and TFA provides the carbonyl. Yaghi and co-workers reasoned that MOF-48, a MOF featuring structurally well-defined 1D oxy-vanadium(IV) chains as nodes and presenting hydrophobic microporous channels (**Figure 18**), might also catalyse methane conversion to acetic acid.[172] This indeed is the case, but now with methane supplying both carbons (as established by ^{13}C NMR measurements of liquid-phase product obtained with $^{13}CH_4$). The net reaction at 80 °C is shown as **eq. 5**:

$$2\ CH_4 + 2\ H_2O + 4\ S_2O_8^{2-} \rightarrow CH_3COOH + 8\ HSO_4^{1-} \qquad (5)$$

Notably, MOF-48 outperforms MIL-47, a closely similar MOF that lacks linker-based methyl groups, so contains channels that are less hydrophobic. For both MOFs, the yield for acetic acid is modest (70% or less, depending on specific conditions and on how yield is defined). One source of yield attenuation is the methylation of TFA to give CF_3COOCH_3. Although the authors did not report on gas-phase products, another source of attenuation may be methane conversion to free CO and possibly CO_2.

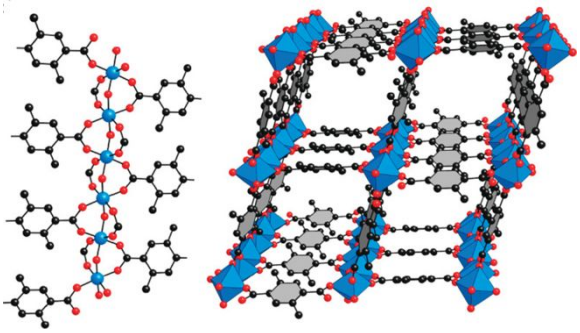

Figure 18. (Left) 1D oxy-vanadium(IV) chains as nodes in MOF-48, and (Right) MOF-48 with 1D hydrophobic microporous channels. Color code: V, blue; O, red; N, dark blue; C, gray. Adapted with permission from Ref. 172. Copyright 2011 American Chemical Society.

2.2.4 Oxidative Coupling to Form Ethylene

Ethylene is among the most widely used building blocks for polymers and for commodity chemicals.[173] In principle, ethylene is accessible from methane (**eq. 5**) *via* reaction with O_2 in a process that is thermodynamically favourable. In practice, it has yet to be commercialized at scale. The reaction typically proceeds through methyl radicals, obtained by overcoming a *ca.* 440 kJ/mol bond dissociation energy *via* hydrogen abstraction by O^{2-} sites of metal-oxide catalysts. A typical reaction temperature, in the presence of a metal-oxide catalyst, is 800 °C – a temperature at which loss of selectivity due to over-oxidation is essentially unavoidable, without sacrificing yield.[117] Furthermore, 800 °C is well above the highest reported temperature for MOF stability (*i.e.*, ~ 500 °C)[174]. Of note, Siluria has reportedly been able to lower the reaction temperature by using proprietary "nanowire" catalysts and to lift reaction yields *via* multi-stage reactor schemes.[175] To our knowledge, there are, as yet, no experimental examples of MOF-catalysed ethylene formation *via* **eq. 6**.

$$2\ CH_4 + O_2 \rightarrow C_2H_4 + 2\ H_2O \qquad (6)$$

2.2.5 Selective Mono-Borylation of Methane

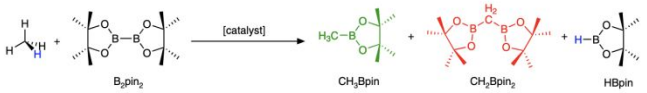

Schematic Figure 19. Methane borylation with B_2pin_2 to yield both mono- and diborylated methane. Adapted with permission from Ref. 182. Copyright 2018 Springer Nature.

Borylation reactions offer an alternative means of exploring and understanding selective C-H bond activation. Furthermore, the borylated products can be used as stepping stones or synthons for more complex compounds.[176] Selected iridium complexes can accomplish hydrocarbon borylation.[177-179] Cook *et al.* and Smith *et al.* reported on homogeneous catalysts that preferentially borylate methane over cyclohexane, even in cyclohexane as solvent – intriguing findings given both the concentration differences and the stronger C-H bond for methane.[180, 181] These catalysts tend,

however, to yield both mono- and diborylated methane; see **schematic Figure 19**.

Figure 20. Preparation of a functional methane-borylation catalyst, UiO-67-Mix-Ir, by

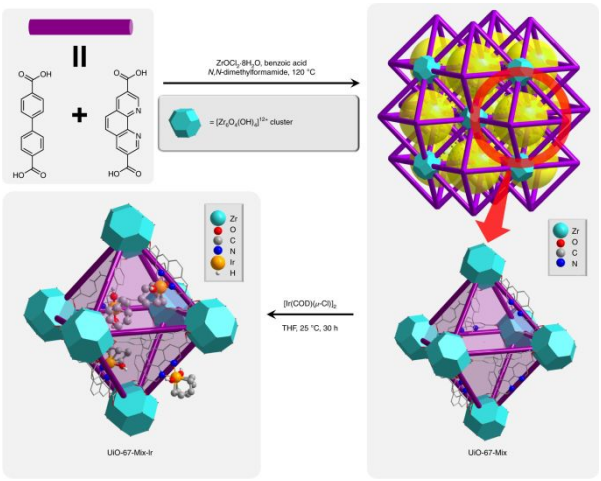

doping with phenanthroline-dicarboxylate as a size-matched linker in UiO-67 and then deploying the doped linker as a chelating ligand for an iridium catalyst. The purple rods and turquoise truncated octahedra represent the linkers and nodes, respectively. The large yellow spheres are a visual indication of the octahedral cavities in UiO-67-Mix. Color: orange, Ir; turquoise, Zr; grey, C; blue, N; red, O, and light-grey, H. Adapted with permission from Ref. 182. Copyright 2018 Springer Nature.

Zhang and coworkers[182] showed that a functional methane-borylation catalyst could be incorporated in the Zr-MOF, UiO-67 (Zr.NEQFBGHQPUXOFH.MOFkeyv1.fcu), by doping with phenanthroline-dicarboxylate as a size-matched linker (in place of biphenyl-dicarboxylate)[113] and then deploying the doped linker as a chelating ligand for an iridium catalyst; see **Figure 20**. Their aim was to exploit catalyst confinement together with MOF-aperture-defined shape-selectivity for delivery of methane versus CH_3Bpin to the catalyst, thereby inhibiting diborylation. After optimization (150 °C, dodecane solvent), they observed a greater than 99% preference for catalytic mono-borylation over di-borylation. In addition to facilitating methane solubility, dodecane itself can be borylated, and thus serves as an additional competitor to CH_3Bpin as a reactant. Indeed, in the presence of the MOF-immobilized catalyst, about 80% of the initially present borylating agent, B_2pin_2, reacts with dodecane, with the remaining 20% reacting with methane to form CH_3Bpin. A follow-up study from the same group showed the mechanistic investigation of this borylation system using benzene as a model substrate.[183] In a computational study, Truhlar and co-workers[184] refined the explanation for the high selectivity of MOF-confined catalyst for production of mono-borylated methane. Briefly, they showed that both methane and CH_3Bpin can be catalytically borylated, but that very slow transport of CH_3Bpin through framework apertures, relative to methane transport through apertures, accounts for much of the selectivity for mono-borylated methane.

Lin and co-workers[185] reported the installation of mononuclear iridium(III) complexes in a high-stability Zr-MOF that presents spatially isolated tri-aryl phosphine sites (linker components) suitable for monodentate ligation of Ir(III); see **Figure 21**. The material is selective for catalytic mono-borylation of methane at 110 °C. Notably, it displays higher catalytic activity and much greater stability than a homogeneous analogue. The authors showed that these advantages accrue from inhibition of destructive disproportionation and iridium nanoparticle formation. They further showed that the most active form of the catalyst, *i.e.* a monophosphine species formed within the MOF and featuring a uniquely low coordination number, cannot be obtained in homogeneous solution.

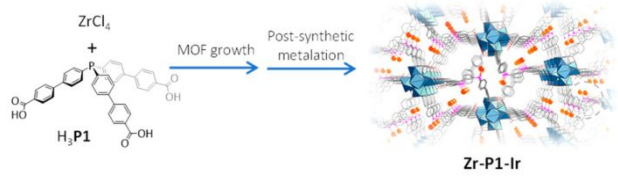

Figure 21. Installation of mononuclear iridium(III) complexes in a high-stability Zr-MOF that presents spatially isolated tri-aryl phosphine sites (linker components). Adapted with permission from ref. 185. Copyright 2019 American Chemical Society.

2.3 Conversion of C_2 Hydrocarbons

2.3.1 Selective Partial Oxidation to Ethanol

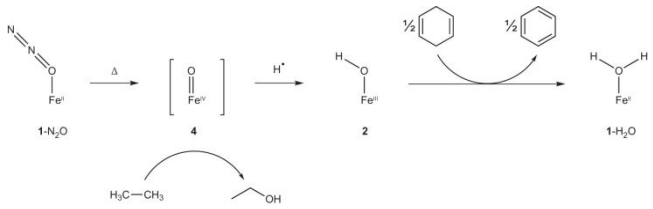

Schematic Figure 22. Heating of N_2O-bound Fe_2(dobdc) (**1**-N_2O) to 60 °C results in the formation of a transient high-spin Fe(IV)–oxo species (**4**), which can react with the strong C–H bonds of ethane. In the absence of a hydrocarbon substrate, the Fe(IV)–oxo quickly decays via hydrogen-atom abstraction into an Fe(III)–hydroxide (**2**), which is isolable and well characterized. This hydroxide species can react with weak C–H bonds, such as those in 1,4-cyclohexadiene, to form benzene and H_2O-bound Fe_2(dobdc) (**1**-H_2O). Adapted with permission from ref. 186. Copyright 2014 Springer Nature.

Xiao and co-workers[186] have reported that a mixed metal MOF, $Fe_{0.1}Mg_{1.9}$-MOF-74, can facilitate the selective conversion of ethane to ethanol using N_2O as the oxidant in a batch reactor (TON = 1.6, ethanol : acetaldehyde = 25:1, products were extracted by CD_3CN) (**Table 2**). In contrast, pure MOF-74(Fe), with its high density of Fe sites, understandably exhibits a propensity for reactant over-oxidation. Extensive Mössbauer spectroscopy, powder X-ray diffraction (PXRD), and neutron diffraction studies showed that exposing five-coordinate Fe(II) sites to N_2O can yield six-coordinate (octahedral) Fe(III)-OH sites – potential precursors to highly active, unstable Fe(IV)=O species. Consistent with the notion of transient formation of reactive Fe(IV)=O sites, exposure of ethane and N_2O to heterogenized Fe(II) sites (in MOF-74) yielded ethanol and Fe(III)-OH (in MOF-74), see **Figure 22.** DFT calculations supported the feasibility of transient generation of a high-spin (S=4) Fe(IV)=O – behaviour facilitated by the weak ligand field generated by carboxylate-coordination.[187, 188] In contrast to most non-heme Fe(IV)-oxo catalysts, which feature triplet ground states, a quintet ground state for the MOF-74 based Fe(IV)-oxo permits the reaction with ethane to occur on a single spin surface without additional barriers for spin crossover. Rather than C-H activation, the cleavage of the N–O bond

in N_2O to create Fe(IV)=O species is the rate-determining step. A TON slightly higher than one points to quasi-catalytic behaviour, with slow desorption rate of EtOH. As noted in the section on C_1 chemistry, theoretical studies showed that increasing the electron-donating ability of the linker can lower the energy barrier for the generation of active Fe(IV)=O species.[160, 189]

Despite their practical limitations, studies of MOF-node-facilitated stoichiometric transformations of alkanes, followed by product extraction and reaction repetition, can be advantageous for: a) obtaining high yields and high selectivity for alcohol products, b) spectroscopically observing mechanistically significant moieties that are otherwise only transiently present, c) observing and understanding catalyst evolution, and d) spectroscopically interrogating species and processes responsible for "catalyst" deactivation.

2.4 Conversion of C_3 Hydrocarbons

2.4.1 Partial Oxidation (Oxygenation) of Propane

Experimental studies of MOF-catalyst-facilitated oxygenation of propane are comparatively few and appear to be limited to ones employing N_2O. As illustrated by the mechanism proposed in **Figure 23**, MIL-100(Fe) (Fe.QMKYBPDZANOJGF.MOFkey-v1.moo) is catalytically competent for partial oxidation of propane.[190] As noted above, the node of MIL-100(Fe) features two Fe(III) centres and one high-spin Fe(II) centre linked by a single oxo ion. When heated, the Fe(II) centre can eliminate a ligand, thereby opening a coordination site capable of binding and activating N_2O, subsequent loss of N_2 being the rate-determining step for the overall catalytic reaction. The pair of Fe(III) centres behave only as spectators, as convincingly shown by Simon and co-workers by selectively poisoning Fe(II) with NO. The study additionally revealed that, within experimental uncertainty, every Fe(II) site in MIL-100(Fe) is reactant accessible and catalytically competent – a finding that underscores the value of working with uniformly porous and atomically well-defined, crystalline materials as catalysts.

The resulting Fe^{IV}=O moiety is a potent oxidant, as evidenced, in part, by the formation of both 1-propanol and 2-propanol as products. Also formed and detected in solution are acetone, and 1,2- and 1,3-propane diol. Double oxidation is not unexpected, as singly oxidized products can encounter enormous numbers of tri-iron nodes as they navigate MOF pores.

Consistent with the above description regarding rate-limiting N_2O fragmentation, reaction rates are zeroth-order in propane. DFT calculations point to a radical rebound mechanism for conversion of propane to propanol. For the initial stages of the reaction (oxidant activation) DFT calculations yield an activation energy that agrees with the activation energy determined experimentally from rate measurements as a function of temperature.

For MIL-100, an especially attractive experimental feature that lends itself well to computationally guided catalyst design is the extent to which node metal-ion composition can be varied within a common structural motif. Additional DFT work suggested that replacing the spectator Fe(III) sites with Al(III) or Cr(III) within the tri-iron clusters of MIL-type MOFs can strongly impact the N_2O activation energy on Fe(II) sites.[166] With this in mind, Barona and co-workers extended (computationally) the node metal-ion composition to a range of first-row transition metals and calculated the corresponding reaction energetics – albeit, for methane and ethane rather than propane.[165] They found that transfer of electron density from spectator metal ions to the active metal ion facilitates N_2O activation. On this basis, Cr_3 and Cr_2Fe were identified as top candidates for catalysis of alkane oxidation.

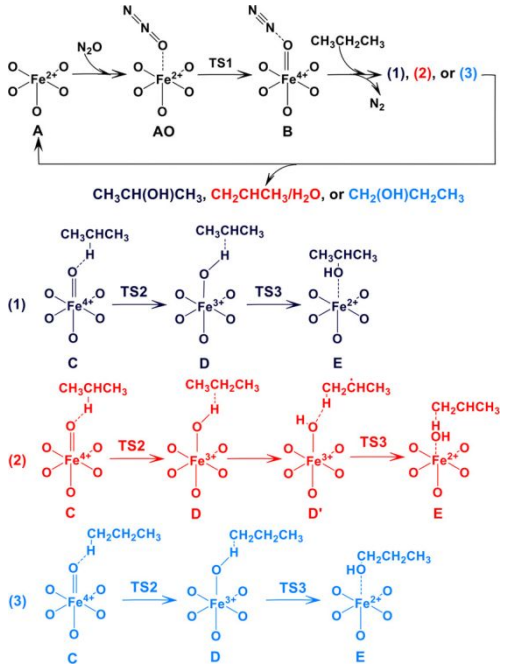

Figure 23. Catalytic cycles for propane conversion to 2-propanol, propylene, and 1-propanol on Fe(II) sites in MIL-100(Fe). Adapted from Ref. 190. Copyright 2019 American Chemical Society.

2.4.2 Dehydrogenation

Dehydrogenation of ethane or propane (**eq. 7**) converts the alkane from a low-value fuel to a higher value, polymerizable building block. For linear alkanes, the process is highly endothermic, meaning that high temperatures (too high for MOF use) are required and that catalyst inactivation by coking (carbon deposition due to excessive dehydrogenation) can occur.

$$2\ CH_3CH_2CH_3 \rightarrow 2\ CH_3CHCH_2 + H_2 \qquad (7)$$

The reaction temperature can be lowered and the reaction made much less endothermic by introducing O_2 and forming H_2O rather than H_2 as a by-product (**eq. 8**):

$$2\ CH_3CH_2CH_3 + 0.5\ O_2 \rightarrow 2\ CH_3CHCH_2 + H_2O \qquad (8)$$

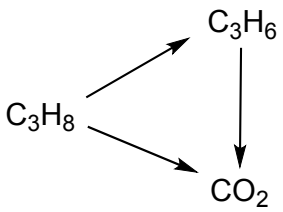

Schematic **Figure 24**. Illustration of the competition of propene formation with combustion reaction, either *via* propene combustion or *via* propane combustion.

Competing reactions are combustion, either of the alkane reactant or the alkene product; see Schematic **Figure 24**. Based on this simple

scheme, lower temperatures typically favour better yields, while higher temperatures increase overall catalytic activity. Thus, an ongoing challenge is to develop catalysts that exhibit significant activity at temperatures low enough to be reasonably selective for oxidative dehydrogenation (ODH).

2.4.2.1 Oxidative Dehydrogenation Using O_2

Li *et al.*[191] showed that cobalt(II)-oxy clusters could be grafted to the hexa-zirconium(IV)-oxy nodes of the MOF, NU-1000, at sites presenting reactive aqua and/or hydroxo ligands. Grafting was accomplished by a process akin to ALD, termed AIM (**A**LD **i**n **M**OFs). Briefly, mononuclear (molecular) cobalt species were heated to *ca.* 120 °C to achieve volatility, permeate the MOF pores, and react in self-limiting fashion with node-sited O-H groups. The installed, partially reacted, precursor complexes were then treated with steam, at 125 °C, to remove remaining precursor ligands and add aqua or hydroxo ligands to cobalt(II). At this temperature, the installed oxy-cobalt species consolidate to form tetra-nuclear cobalt(II)-oxy clusters, sited and node-grafted exclusively in the ~8 Å diameter *c*-pores that cross-connect trigonal (small) and hexagonal (large) channels. Each cluster is grafted to, and spans, a pair of MOF nodes. Difference envelope density (DED) maps obtained from "before" and "after" X-ray scattering data, where a synchrotron provides the needed X-ray intensity, shows cluster siting in MOFs; see **Figure 25**.

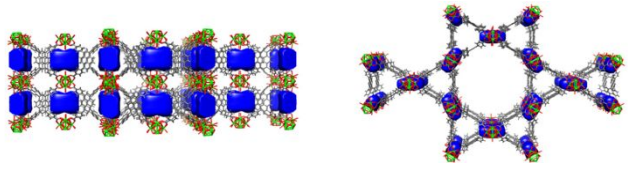

Figure 25. DED of Co-AIM+NU-1000. The side view (Left) is perpendicular to the *a*–*b* plane of NU-1000 and the top view (Right) is in the *a*–*b* plane of NU-1000. Adapted from Ref. 191. Copyright 2017 American Chemical Society.

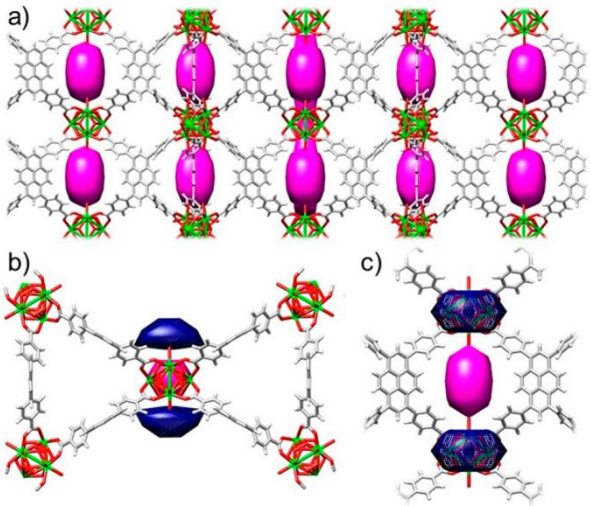

Figure 26. DED maps of (a) NDC-NU-1000 along the *a*-axis, and (b) Co-NDC-NU-1000 viewed along the MOF crystallographic *c*-axis, and (c) *a*-axis. Electron density taken from the subtraction of NU-1000 from NDC-NU-1000 is shown in magenta. Electron density envelopes attributed to Co^{2+} ions are shown in blue and taken from the subtraction of NDC-NU-1000 from Co-NDC-NU-1000. Adapted from Ref. 75. Copyright 2018 American Chemical Society.

Peters and co-workers[75] showed that the siting of catalytically competent cobalt ions on the nodes of NU-1000 can be directed away from the *c*-pore and exclusively into the MOF's mesopores; see **Figure 26**. The approach capitalizes upon the ability to place auxiliary linkers into a framework, with crystallographic precision. While the redistribution of active sites had little effect upon catalysis of oxidative dehydrogenation of vapor-phase propane, it does have general utility as a way of controlling the metal nuclearity of installed active sites.[136] Relative to zeolites, and especially for vapor-phase chemical transformations, the notion of local environmental control near the catalyst active-site within MOFs is arguably an underexplored idea.[85, 167]

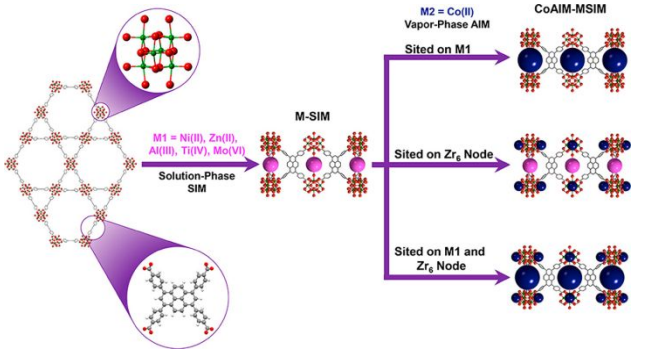

Figure 27. Schematic representation of the preparation of the NU-1000-supported bimetallic catalysts. The promoter ions are anchored *via* SIM (pink) and Co ions are anchored *via* AIM (blue). Adapted from Ref. 58. Copyright 2017 American Chemical Society.

Li and co-workers[58] showed that nodes can be functionalized in stepwise fashion with pairs of metal oxides of differing chemical composition. On this basis, they were able to install oxy-cobalt catalysts on MOF nodes that had already been modified with oxy-Ni(II), -Zn(II), -Al(III), -Ti(IV), or -Mo(VI) clusters. **Figure 27** shows a DED-determined representation of the arrangement of successively installed oxy-Ni(II)/Zn(II)/Al(III)/Ti(IV)/Mo(VI) and oxy-Co(II) clusters. The initially installed clusters behave as promoters, with the activity of the Co(III)-oxy-cluster based dehydrogenation catalyst systematically increasing with decreasing Lewis acidity of the promoter. Dehydrogenation is facilitated by Co(III)–O• (oxyl) formation, with the promoter serving to tune electron density on the oxygen radical. Simons *et al.*[192] have reported on computational studies of closely related, MOF-node-supported, mixed-metal-oxide clusters, and arrived at mechanistic conclusions consistent with those put forward by Li *et al.* in their experimental studies.

As suggested by the DED data in **Figures 25-27**, thermal disorder accompanying the highly exothermic, two-step AIM process, and aggravated by the generally poor thermal conductivity of channel-evacuated MOFs, precludes atomic resolution of cluster structure, but does permit resolution on the few to several angstrom length-scale. The addition of PDF (pair distribution function) data from total X-ray scattering, along with EXAFS, and electronic structure calculations to rank stabilities of candidate structures for clusters, provide an informed representation of the likely structure. Recall that EXAFS and PDF experiments can yield coordination numbers and atom-atom separation distances, when short-range order and site-uniformity exist; long-range order (crystallinity) is not a requirement.

Thus, quantitative structural information can be collected for arrays of MOF-supported catalysts that are sited, for example, with a range of orientations, but are otherwise uniform.

2.4.2.2 Oxidative Dehydrogenation Using N_2O

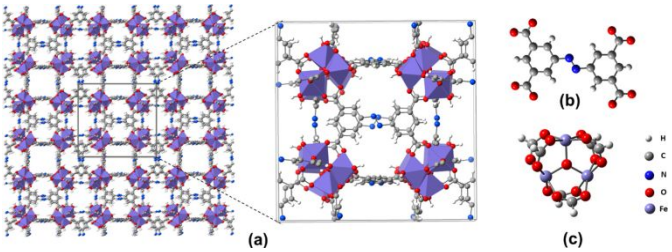

Figure 28. (a) Crystallographic structure of PCN-250(Fe_3) and its unit cell, (b) its ABTC linker (ABTC = 3,3′,5,5′-azobenzenetetracarboxylate), and (c) node cluster representation of $Fe_3(\mu_3\text{-}O)(COO)_6$ terminated with hydrogen atoms. Adapted from Ref. 193. Copyright 2019 American Chemical Society.

As noted above, MIL-100(Fe) catalyses the oxidation of propane by N_2O and yields a mix of oxygen-containing, liquid-phase products, evidently *via* a radical rebound mechanism (**Figure 23**). Curiously, analysis of the reaction vapor-phase revealed the formation of propylene in remarkably high yield, *i.e.* >40%. While not an oxygenated product, propylene is an oxidation product. Its detection here is indicative of a partial departure from typical radical-rebound pathways; two consecutive hydrogen atom abstraction (HAA) steps are necessary for desaturation. DFT studies suggest that the second HAA is kinetically more favourable than alkyl rebound to oxyl to produce alcohols. DFT-based modelling also indicated a lower barrier for desorption of propylene than for desorption of any of the alcohol products.

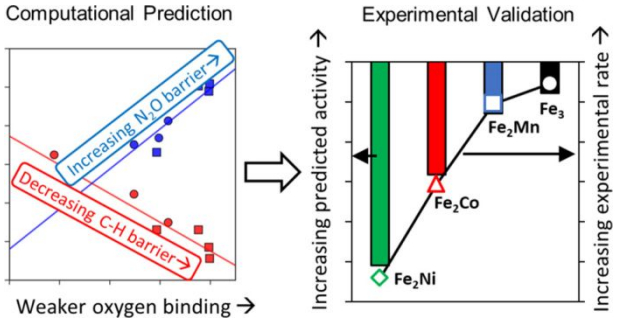

Figure 29. Computational prediction and experimental validation match each other on alkane oxidative dehydrogenation by Fe_2M MOF nodes of PCN-250. Adapted from Ref. 193. Copyright 2019 American Chemical Society.

Barona *et al.*[193] computationally examined the oxidative dehydrogenation of propane (and cyclohexane) by N_2O as catalysed by the mixed-metal nodes of PCN-250(Fe_2M) (Fe_3: Fe.MXBBZODCMBYDCL.MOFkey-v1.soc), **see Figure 28** for crystallographic structure. Additionally, they experimentally examined catalytic ODH of cyclohexane (primarily to cyclohexene). The authors point out that cyclohexane is an experimentally convenient surrogate for linear alkanes because only one type of C-H bond is present. Since N_2O activation barrier is higher than the C-H activation barrier, N_2O activation is the rate-determining step. Further experimental study of the vapor-phase oxidation of cyclohexane using a series of PCN-250 (Fe_2M, M=Fe, Mn, Co, Ni) MOFs followed the same reactivity trend as the computational study predicted (**Figure 29**). This work underscores the potential for synergy between computational and experimental efforts.

2.5 Conversion of C_4 Hydrocarbons

n-Butane is used to make maleic anhydride, and has, at times, also been used to make 1,3-butadiene, *via* dehydration, but at temperatures too high to be compatible with MOF-based catalysts.[194-195] Separation of n-butane from other n-alkanes and from isobutane has been demonstrated with MOFs as sorbents.[196] The selective formation of the C_4 species, 1,3-butadiene from acetylene,[68] and 1-butene + 2-butene from ethylene,[85] *via* MOF-supported catalysts has been described, as have the isomerization and the hydrogenation of 1-butene, and the dimerization of isobutene.[81, 197] Among other mechanistically intriguing catalytic phenomena, the reports describe, specifically for zirconia-like MOF nodes, heterolytic dissociation of molecular hydrogen, as well as sulfation-facilitated super-acid or near-super-acid behaviour. To our knowledge, however, no experimental studies of MOF-catalysed transformations of n-butane itself have been reported.

Nevertheless, a series of computational studies of MOF-pore-enabled, selective partial oxidation of n-butane to n-butanol have been described.[198-201] The proof of concept comes from experimental studies of regioselective hydrogenation of alkenes catalysed by ZIF-8 (Zn.YFFQUDCLMWOYCW.MOFkey-v1.sod) enshrouded Pt nanoparticle.[202] The key finding was that hydrogenation could be sterically limited to terminal C=C bonds; see **Figure 30**. The significant conclusion was that MOF pores can control alignment and interfacial-access of candidate reactants on the few-atom scale. The computational studies focus on Ag_3Pd nanoparticle and related alloy catalysts enshrouded by ZIF-8 and related materials.[203] A defining feature of ZIF-8 is the presence of pore apertures that can expand and contract in hinge-like fashion (six Zn(II)-hinged methyl-imidazolate linkers per apertures) to admit candidate reactants into pores or to enable their diffusive transport from one pore to another.[204-207] By analogy to hydrogenation studies, the authors hypothesized that at the interface of the MOF and the catalytic metal nanoparticle, oxidation (oxygenation) can be limited to a terminal carbon of a linear alkane. Follow-up computational studies focused on microkinetic modelling as a means of selecting conditions for optimal chemical selectivity.[203] To our knowledge, experimental tests of this interesting work have yet to be published.

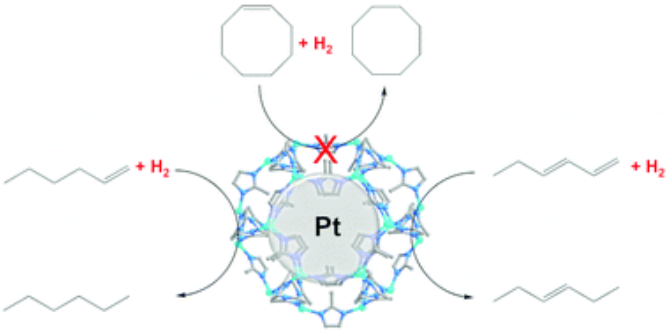

Figure 30. ZIF-8 apertures admit 1-hexene, but block cis-cyclooctene – behaviour that translates into selective catalytic hydrogenation of the linear compound. Adapted with permission from ref. 200. Copyright 2015 Royal Society of Chemistry.

3. Conclusions and Outlook

Arresting climate change may well prove to be the defining scientific challenge of this century. No doubt, at the forefront will be decarbonization. Just as combustion of coal and oil for heating and electrical power generation have been increasingly supplanted by cleaner and more efficient combustion of natural gas, renewable, carbon-free energy sources will replace natural gas. Likewise, electrochemical and/or photoelectrochemical water splitting will almost certainly supplant methane steam-reforming as the main route to H_2, both as an increasingly viable energy carrier and as the input for massive production of ammonia, essential for efficient plant-based food production. The need for carbon-based *materials*, however, will outlive the need for carbon-based fuel and the need for methane-derived molecular hydrogen.

Historically derived by first cracking petroleum to form naphtha (C_5-C_{10} mixtures), the building blocks for carbon-based polymers are increasingly obtained by processing the wet components (C_2, C_3, and C_4 components) of shale gas. Indeed, in regions where fracking has enabled access to enormous reserves of wet shale gas, building up and/or converting these feedstocks to manufacturing-relevant commodity chemicals has largely supplanted the breakdown of long-chain hydrocarbons and alkyl-linked polyaromatics as the source for feedstocks. When "building up" replaces "breaking down" as a chemical starting point, the initial catalytic chemistry shifts from the high-temperature regime (*ca.* 500 to 750 °C for fluid catalytic cracking of petroleum[3]) to more modest temperatures. The shift to lower operating temperatures obviously also lowers the ceiling for thermal stability of catalysts. In turn, crystallographically well-defined MOFs become viable as model catalysts and model catalyst-supports. Their broad structurally tunability and their amenability to structural characterization, including *operando* characterization and post-catalytic characterization, facilitates theory-guided, hypothesis-driven investigations of activity and selectivity. Ideally, the resulting chemical insights and understanding will prove transferable to other catalyst platforms.

MOF constructs and hydrocarbon-relevant catalytic activity. In our view, underexplored in MOF chemistry is the formation of well-defined and uniformly sited oxygen vacancies in node-based metal-oxide units, *e.g.* oxy-M_3, oxy-M_6, oxy-M_{12} units, as well as in extended periodic rod-like oxy-metal nodes. With their propensity to activate molecular oxygen and thereby lower activation energies and temperatures for desired oxidative catalytic transformations, vacancies are especially attractive catalyst constructs. MOF-node-based catalysts would seem to hold out the possibility of directly observing and fully structurally characterizing activated, vacancy-occupying, but not yet reacted, di-oxygen species. This level of characterization could be a boon to mechanistic understanding and to computationally guided design of superior catalysts or deployment of existing catalysts. Experimental and computational elucidation of Mars van Krevelen type oxidative catalysis by MOF-supported oxy-metal clusters provides support for this idea. Siting oxygen vacancies directly on MOF nodes could enable extensive contact with separately installed, reactant-accessible, zero-valent metal clusters or nanoparticles, where the interface between the two components would likely define the most useful catalytic sites.

Closely related, but also under-explored, is the exploitation of MOF atomic-scale periodicity/crystallinity, together with high-intensity synchrotron radiation, to observe the staging of gas-phase catalytic reactions under *operando* or near-*operando* conditions. Perhaps easiest to envision is the siting and catalytic evolution of small hydrocarbons as a function of temperature, reactant or chemical-intermediate composition, active-site structure, active-site accessibility, and active-site surrounding environment. Notably, reports on proof-of-concept experiments are starting to appear in the peer-reviewed literature.[208]

In terms of chemical structure and composition, MOFs reside at a conceptual interface between non-molecular inorganic compounds and molecular or supramolecular species. The potential ability of frameworks to organize, orient, and usefully constrain molecule-derived heterogeneous catalysts has been widely recognized. An intriguing idea that has been little explored is the intentional introduction of mechanical strain on MOF-supported or MOF-integrated molecular catalysts *via* the framework itself – for example, by enticing a catalytically active, ditopic molecule to function as a secondary linker and span a distance slightly greater (or slightly less) than preferred by the isolated molecule at rest. With the right system, framework engendered strain would push the active portion of the molecular catalyst toward an metalloenzyme-like entatic state,[209] thereby lowering activation energies and increasing rates.

The mixed organic and inorganic character of MOF materials, together with the synthetic accessibility of topologies that exhibit hierarchical, molecular-scale porosity, points to the potential for creating distinct, but interconnected, hydrophilic and hydrophobic networks. If catalysts are sited at network/network intersections, one could envision delivery of alkane reactants through one network and removal of alcohol products through another. Ideally, if catalyst loading is optimal, MOFs featuring complementary hydrophobic and hydrophilic channels could serve to inhibit over-oxidation of reactants, *via* preferential expulsion of products.

Also little studied, but potentially ripe for investigation is the separation of gas-phase alkane oxidation reactions into condensed-phase electrochemical half-reactions, where the half-reaction of greatest interest would be selective partial oxidation (oxygenation) of dissolved hydrocarbons by electrodes composed of redox-active metal-oxides capable of catalysis based on interfacial transfer of oxygen atoms. High-temperature solid-oxide fuel cells (SOFCs) accomplish something akin to this idea, when they employ alkanes as fuels.[210-212] With fuel cells, the goal is to generate the maximum amount of electrical power; consequently, complete oxidation to CO_2 is much more desirable than partial oxidation. In contrast, the goal in an electrocatalytic synthesis cell would be selective partial oxidation. Independent control of the applied electrochemical potential might provide a basis for suppressing over-oxidation, with the role of a MOF coating being to preconcentrate and suitably orient a reactant to optimize activity and selectivity. Thus, in this scenario the MOF itself

would be catalytically passive, but essential for facilitating electrocatalytic selectivity.[213]

C_1-C_4 reactivity. While wet shale gas, by definition, contains significant amounts of C_2, C_3, and C_4, the majority – typically 85% or higher – is methane. An effective, carbon-efficient, and moderate temperature (< 400 °C) route from methane to methanol, based on O_2 as the oxidant, has yet to be demonstrated for MOF-based or MOF-supported catalysts. If such a route could be discovered, and then translated to inherently more robust platforms, it would be transformative. Perhaps the recent finding that the active methane-monoxygenase employs a single copper ion will be the key to altering the designing of artificial catalysts and functionally mimicking pMMO. Or, perhaps attention will turn to catalysis inspired by the diiron active-sites of soluble MMO.[153] Supportive of the notion that such studies will prove enlightening are findings from recent studies of conversion of ethane to ethanol *via* MOF-sited, iron-containing catalysts; these studies made use of N_2O as an oxidatant.[186, 187]

C_3, and presumably C_4, can be catalytically transformed by MOF-supported catalysts from low-value alkane to high-value olefin species *via* moderate temperature (*ca.* 200 °C) oxidative dehydrogenation using O_2 as a co-reactant. Similar MOF-enabled chemistry has yet to be demonstrated for conversion of ethane to ethylene. The dominant commercial route to ethylene from ethane is thermal cracking, where the endothermic character of the transformation mandates high reaction temperatures – too high to be compatible with MOFs. Unfortunately, thermal cracking of ethane to form ethylene and H_2, is an inherently energy intensive process. By coupling alkane dehydrogenation to formation of water, using O_2 as the oxygen source, the transformation becomes exothermic and susceptible, therefore, to execution at much lower temperature, with exothermicity of the transformation itself providing much of the heat needed to drive the reaction at an acceptable rate. A major challenge catalytically is to run the reaction rapidly, but at low enough temperature that formation of CO_2 (from either ethane or ethylene) can be largely suppressed. Significant progress has been made in understanding and demonstrating, at much lower temperatures (*ca.* 400 °C), selective ODH of ethane *via* metal-oxide based catalysts.[214] It is worth considering how MOF-supported catalysts, with their characteristic uniformity and well-defined structures and compositions, might be exploited to broaden catalyst discovery and potentially push this chemistry further toward practical viability.

An alternative to MOF-based catalysts. Finally, for substantially endothermic reactions or for other reactions that push or exceed the upper limits of MOF thermal stability, a potentially promising alternative approach may be to employ as catalysts, MOF-pyrolysis-derived, graphene/graphite-like materials featuring nitrogen doping and in-plane coordination of transition-metal ions,[215, 216] as these can withstand prolonged exposure at higher temperatures. Lost with pyrolysis, however, is well-defined structural periodicity, well-defined porosity, and to a large extent, crystallinity. Nevertheless, surface areas can be nearly as large as those of typical MOFs, and local structural information about catalytic metal sites, *e.g.* coordination number, coordination environment and uniformity of environment, metal nuclearity, metal-nitrogen bonds lengths, and metal atom oxidation state, can be obtained *via* synchrotron-based XAS and XRD measurements. Further, these materials offer admirably large thermal and electrical conductivity, especially relative to most, if not all, MOFs.

Table 1. MOFid and MOFkey of all MOFs mentioned in this review. For CIFs containing disorder that significantly affects the generation of MOFids and MOFkeys, resulting in structural errors, they are excluded from the table.

MOF Name	MOFkey	MOFid
MOF-808	Zr.QMKYBPDZANOJGF.MOFkey-v1.spn	O[Zr]123([OH2])[OH]4[Zr]56([O]3[Zr]37([OH]2[Zr]28([O]1[Zr]14([O]6[Zr]([OH]53)([OH]21)([O]78)([OH2])O)([OH2])(O)O)[OH2])([OH2])(O)O)[OH2].[O-]C(=O)c1cc(cc(c1)C(=O)[O-])C(=O)[O-] MOFid-v1.spn.cat0
NU-1000(Zr)	Zr.HVCDAMXLLUJLQZ.MOFkey-v1.csq	O[Zr]123([OH2])[OH]4[Zr]56[O]3[Zr]37([OH]2[Zr]28[O]1[Zr]14([O]6[Zr]([OH]53)([OH]21)([O]78)([OH2])O)([OH2])O)([OH2])O.[O-]C(O)c1ccc(cc1)c1cc(c2ccc(cc2)C(O)[O-])c2c3c1ccc1c3c(cc2)c(cc1c1ccc(cc1)C(O)[O-])c1ccc(cc1)C(O)[O-] MOFid-v1.csq.cat0
MIL-53(Al)	Al.KKEYFWRCBNTPAC.MOFkey-v1.rna	[Al].[O-]C(=O)c1ccc(cc1)C(=O)[O-].[OH] MOFid-v1.rna.cat0
MIL-53(Al, Fe)	Fe.KKEYFWRCBNTPAC.MOFkey-v1.rna	[Fe].[O-]C(=O)c1ccc(cc1)C(=O)[O-].[O] MOFid-v1.rna.cat0
UiO-66(Zr)	Zr.KKEYFWRCBNTPAC.MOFkey-v1.fcu	[O-]C(O)c1ccc(cc1)C(O)[O-].[O]12[Zr]34[OH]5[Zr]62[OH]2[Zr]71[OH]4[Zr]14[O]3[Zr]35[O]6[Zr]2([O]71)[OH]43 MOFidv1.fcu.cat0
MOF-74(Fe)	Fe.YXUXCIBWQAOXRL.MOFkey-v1.etb	[Fe].[O-]C(=O)C1=CC(=O)C(=CC1=O)C(=O)[O-] MOFid-v1.etb.cat0
MIL-101(Fe)	Fe.KKEYFWRCBNTPAC.MOFkey-v1.mtn-e	F[Fe][O]([Fe])[Fe].[O–]C(O)c1ccc(cc1)C(O)[O–] MOFid-v1.mtn-e.cat0
MOF-48	V.FKUJGZJNDUGCFU.MOFkey-v1.rna	[O-]C(=O)c1cc(C)c(cc1C)C(=O)[O-].[O].[V] MOFid-v1.rna.cat0
UiO-67	Zr.NEQFBGHQPUXOFH.MOFkeyv1.fcu	[O]C(O)c1ccc(cc1)c1ccc(cc1)C(O)[O].[O]12[Zr]34[OH]5[Zr]62[OH]2[Zr]71[OH]4[Zr]14[O]3[Zr]35[O]6[Zr]2([O]71)[OH]43 MOFid-v1.fcu.cat0
MIL-100(Fe)	Fe.QMKYBPDZANOJGF.MOFkey-v1.moo	F[Fe][O]([Fe])[Fe].F[Fe][O]([Fe]F)[Fe].[Fe][O]([Fe])[Fe].[O-]C(O)c1cc(cc(c1)C(O)[O-])C(O)[O-] MOFid-v1.moo.cat0
PCN-250(Fe_3)	Fe.MXBBZODCMBYDCL.MOFkey-v1.soc	O[Fe][O]([Fe]O)[Fe]O.[O-]C(=O)c1cc(N=Nc2cc(cc(c2)C(=O)[O-])C(=O)[O-])cc(c1)C(=O)[O-] MOFid-v1.soc,edq.cat0
PCN-250(Fe_2Co)	FeCo.MXBBZODCMBYDCL.MOFkey-v1.soc	O[Fe][O]([Co]O)[Fe]O.[O-]C(=O)c1cc(N=Nc2cc(cc(c2)C(=O)[O-])C(=O)[O-])cc(c1)C(=O)[O-] MOFid-v1.soc,edq.cat0
ZIF-8	Zn.YFFQUDCLMWOYCW.MOFkey-v1.sod	CC1NCC[N]1.[Zn] MOFid-v1.sod.cat0

Table 2. MOF-based catalysts for selective alkane oxidation to liquids.

Entry	Catalyst	Active Site	P (bar)	T (°C)	Products	Selectivity[a] (%)	Yield/TOF[a,b]	Ref.
1	Cu-NU-1000	Trimeric Cu(II)	1	150	MeOH, DME, CO_2	~ 60	~ 0.03 mol/mol_{Cu}	147
2	Cu-SIM-NU-1000	Dimeric Cu(II)	40	200	MeOH, DME, CO_2	90	0.04 mol/mol_{Cu}	146
3	MIL-53(Al, Fe)	Dimeric Fe(III)	30.5	60	MeOH, methyl peroxide, formic acid, and CO_2	80	90 h^{-1}	153
4	MOF-808-Bzz-Cu	Bis(μ-oxo)dicopper (I)	1	150	MeOH	100	~ 0.02 mol/mol_{Cu}	155
5	MOF-48(V)-180	V(IV) site	20	80	acetic acid	100	24.5 h^{-1}	172
6	$Fe_{0.1}Mg_{1.9}$-MOF-74	Fe(II) site	9	75	EtOH, acetaldehyde	96 (EtOH)	0.067 h^{-1}	186
7	MIL-100(Fe)	Fe(II) site	1.1	120	2-propanol, 1-propanol, acetone, 1,2- and 1,3-propane diol, and propylene	~ 60	N/A	190

a. taking into account of all liquid products; b. calculated on a per-atom basis, even if only a fraction of the active sites are catalytically active.

Abbreviations:

1D	1-dimensional
2D	2-dimensional
3D	3-dimensional
ABTC	3,3′,5,5′-azobenzenetetracarboxylate
AIM	ALD in MOFs
ALD	Atomic layer deposition
B2pin2	Bis(pinacolato)diboron
CIF	Crystallographic information file
CPO	Coordination Polymer of Oslo
DED	Difference envelope density
DFT	Density functionl theory
DME	Dimethyl ether
dodbc	4,4'-dioxido-3,3'-benzenedicarboxylate
EXAFS	Extended X-ray absorption fine structure
HAA	Hydrogen atom abstraction
HB	Hydrogen bond
MAF	Metal-azolate framework
MCM	Mobil Composition of Matter
MIL	Materials Institute Lavosier
MMO	Methane monooxygenase
MOF	Metal-organic framework
MTO	Methanol to olefins
NDC	Naphthalene dicarboxylate
NMR	Nuclear Magnetic Resonance
NU	Northwestern University
ODH	Oxidative dehydrogenation
PCN	Porous Coordination Network
PDF	Pair distribution function
pMMO	Particulate methane monooxygenase
SAPO	Silicoaluminophosphate
SBA	Santa Barbara Amorphous
SCXRD	Single-crystal X-ray diffraction
SIM	Solvothermal deposition in MOFs
sMMO	Soluble methane monooxygenase
SOFC	Solid-oxide fuel cell
TFA	Trifluoroacetic acid
TOF	Turnover frequency
TON	Turnover number
UiO	University of Oslo
XANES	X-ray absorption near edge structure
XAS	X-ray absorption spectroscopy
XRD	X-ray diffraction
ZIF	Zeolitic imidazolate framework
ZSM	Zeolite Socony Mobil

4. Declaration of Competing Interest

The authors declare no competing financial interest.

5. Acknowledgments

We thank Dr. Andrew Rosen for helping generate MOFids and MOFkeys. Work done in our own labs was supported by the Inorganometallic Catalyst Design Center (ICDC), an EFRC funded by the DOE, Office of Basic Energy Sciences (DE-SC0012702), which made use of the EPIC facility of Northwestern University's NUANCE Center receiving support from the Soft and Hybrid Nanotechnology Experimental (SHyNE) Resource (NSF ECCS-1542205); the MRSEC program (NSF DMR1720139) at the Materials Research Center; the International Institute for Nanotechnology (IIN); the Keck Foundation; and the State of Illinois, through the IIN. T. A. G. gratefully acknowledges the support of the U.S. DOE, Office of Science, Office of Workforce Development for Teachers and Scientists, Office of Science Graduate Student Research (SCGSR) program. The SCGSR program is administered by the Oak Ridge Institute for Science and Education (ORISE) for the DOE, and ORISE is managed by ORAU under Contract DE-SC0014664.

6. References

1. N. E. Lauer, J. C. Hower, H. Hsu-Kim, R. K. Taggart, A. Vengosh, *Environ. Sci. Technol.* 2015, **49**, 11227-11233.
2. National Academies of Sciences and Medicine, 2016. *The Changing Landscape of Hydrocarbon Feedstocks for Chemical Production: Implications for Catalysis: Proceedings of a Workshop*. Washington, DC: The National Academies Press.
3. P. J. M. Linstrom, W. G., ed., *NIST Chemistry WebBook, NIST Standard Reference Database Number 69*, National Institute of Standards and Technology, Gaithersburg, MD 20899.
4. E. T. Vogt and B. M. Weckhuysen, *Chem. Soc. Rev.*, 2015, **44**, 7342-7370.
5. Y. Liu, D. Deng and X. Bao, *Chem.*, 2020, **6**, 2497-2514.
6. C. A. Koval, J. Lercher, S. L. Scott, G. W. Coates, E. Iglesia, R. M. Bullock, T. F. Jaramillo, M. Flytzani-Stephanopoulos, D. Resasco, C. L. Tway, V. Batista, K. W. Chapman, S. Dai, J. Dumesic, C. Friend, R. Hille, K. Johnson, J. Nørskov, J. Rekoske, R. Sarkar, C. Bradley, B. Garrett, C. Henderson, R. Miranda, C. Peden, V. Schwartz, K. Runkles, K. Fellner, C. Jenks, M. Nelson, A. M. Appel, S. Bare, B. M. Bartlett, T. Bligaard, B. D. Chandler, R. J. Davis, V.-A. Glezakou, J. Gregoire, R. Hille, A. S. Hock, J. Kitchin, H. H. Kung, R. Rousseau, A. D. Sadow, R. E. Schaak, W. J. Shaw, D. J. Stacchiola, M. Delferro, E. Bunel, J. Holladay, F. Houle, C. Jenks, T. Krause, C. Marshall, N. Neale, J. Parks, J. Schaidle, J. VandeLagemaat, Y. Wang and R. Weber, *Basic Research Needs for Catalysis Science to Transform Energy Technologies*, U.S. Department of Energy, Office of Basic Energy Sciences, Gaithersburg, MD, 2017.
7. M. Dusselier and M. E. Davis, *Chem. Rev.*, 2018, **118**, 5265-5329.
8. R. T. Hannagan, G. Giannakakis, M. Flytzani-Stephanopoulos and E. C. H. Sykes, *Chem. Rev.*, 2020, **120**, 12044-12088.
9. T. Zhang, A. G. Walsh, J. Yu and P. Zhang, *Chem. Soc. Rev.*, 2021, **50**, 569-588.
10. A. Han, B. Wang, A. Kumar, Y. Qin, J. Jin, X. Wang, C. Yang, B. Dong, Y. Jia, J. Liu and X. Sun, *Small Methods*, 2019, **3**.
11. A. Bakandritsos, R. G. Kadam, P. Kumar, G. Zoppellaro, M. Medved, J. Tucek, T. Montini, O. Tomanec, P. Andryskova, B. Drahos, R. S. Varma, M. Otyepka, M. B. Gawande, P. Fornasiero and R. Zboril, *Adv. Mater.*, 2019, **31**, e1900323.
12. A. Ge, B. Rudshteyn, P. E. Videla, C. J. Miller, C. P. Kubiak, V. S. Batista and T. Lian, *Acc. Chem. Res.*, 2019, **52**, 1289-1300.
13. S. W. Sheehan, J. M. Thomsen, U. Hintermair, R. H. Crabtree, G. W. Brudvig and C. A. Schmuttenmaer, *Nat. Commun.*, 2015, **6**, 6469.
14. T. D. Bennett and S. Horike, *Nat. Rev. Mater.*, 2018, **3**, 431-440.
15. M. O'Keeffe and O. M. Yaghi, *Chem. Rev.*, 2012, **112**, 675-702.
16. V. Guillerm, D. Kim, J. F. Eubank, R. Luebke, X. Liu, K. Adil, M. S. Lah and M. Eddaoudi, *Chem. Soc. Rev.*, 2014, **43**, 6141-6172.
17. M. O'Keeffe, M. A. Peskov, S. J. Ramsden and O. M. Yaghi, *Acc. Chem. Res.*, 2008, **41**, 1782-1789.
18. A. Phan, C. J. Doonan, F. J. Uribe-Romo, C. B. Knobler, M. O'Keeffe and O. M. Yaghi, *Acc. Chem. Res.*, 2010, **43**, 58-67.
19. M. Eddaoudi, D. F. Sava, J. F. Eubank, K. Adil and V. Guillerm, *Chem. Soc. Rev.*, 2015, **44**, 228-249.
20. J. P. Zhang, Y. B. Zhang, J. B. Lin and X. M. Chen, *Chem. Rev.*, 2012, **112**, 1001-1033.
21. D. Feng, Z. Y. Gu, J. R. Li, H. L. Jiang, Z. Wei and H. C. Zhou, *Angew. Chem. Int. Ed.*, 2012, **51**, 10307-10310.
22. W. Morris, B. Volosskiy, S. Demir, F. Gandara, P. L. McGrier, H. Furukawa, D. Cascio, J. F. Stoddart and O. M. Yaghi, *Inorg. Chem.*, 2012, **51**, 6443-6445.
23. Y. Chen, T. Hoang and S. Ma, *Inorg. Chem.*, 2012, **51**, 12600-12602.
24. J. E. Mondloch, W. Bury, D. Fairen-Jimenez, S. Kwon, E. J. DeMarco, M. H. Weston, A. A. Sarjeant, S. T. Nguyen, P. C. Stair, R. Q. Snurr, O. K. Farha and J. T. Hupp, *J. Am. Chem. Soc.*, 2013, **135**, 10294-10297.
25. H. Furukawa, F. Gandara, Y. B. Zhang, J. Jiang, W. L. Queen, M. R. Hudson and O. M. Yaghi, *J. Am. Chem. Soc.*, 2014, **136**, 4369-4381.
26. Z. Lu, R. Wang, Y. Liao, O. K. Farha, W. Bi, T. R. Sheridan, K. Zhang, J. Duan, J. Liu and J. T. Hupp, *Chem. Comm.*, 2021, **57**, 3571-3574.
27. W. Lu, Z. Wei, Z. Y. Gu, T. F. Liu, J. Park, J. Park, J. Tian, M. Zhang, Q. Zhang, T. Gentle, 3rd, M. Bosch and H. C. Zhou, *Chem. Soc. Rev.*, 2014, **43**, 5561-5593.
28. M. Eddaoudi, D. B. Moler, H. Li, B. Chen, T. M. Reineke, M. O'Keeffe and O. M. Yaghi, *Acc. Chem. Res.*, 2001, **34**, 319-330.
29. S. Wang, J. S. Lee, M. Wahiduzzaman, J. Park, M. Muschi, C. Martineau-Corcos, A. Tissot, K. H. Cho, J. Marrot, W. Shepard, G. Maurin, J.-S. Chang and C. Serre, *Nat. Energy*, 2018, **3**, 985-993.
30. J. H. Cavka, S. Jakobsen, U. Olsbye, N. Guillou, C. Lamberti, S. Bordiga and K. P. Lillerud, *J. Am. Chem. Soc.*, 2008, **130**, 13850-13851.
31. K. Wang, D. Feng, T. F. Liu, J. Su, S. Yuan, Y. P. Chen, M. Bosch, X. Zou and H. C. Zhou, *J. Am. Chem. Soc.*, 2014, **136**, 13983-13986.
32. J. C. Tan, T. D. Bennett and A. K. Cheetham, *PNAS*, 2010, **107**, 9938-9943.
33. L. Valenzano, B. Civalleri, S. Chavan, S. Bordiga, M. H. Nilsen, S. Jakobsen, K. P. Lillerud and C. Lamberti, *Chem. Mater.*, 2011, **23**, 1700-1718.
34. Z. Lu, J. Liu, X. Zhang, Y. Liao, R. Wang, K. Zhang, J. Lyu, O. K. Farha and J. T. Hupp, *J. Am. Chem. Soc.*, 2020, **142**, 21110-21121.
35. E. Aunan, C. W. Affolter, U. Olsbye and K. P. Lillerud, *Chem. Mater.*, 2021, **33**, 1471-1476.

36. M. Gustafsson, A. Bartoszewicz, B. Martín-Matute, J. Sun, J. Grins, T. Zhao, Z. Li, G. Zhu and X. Zou, *Chem. Mater.*, 2010, **22**, 3316-3322.
37. H. Wang, D. Yu, J. Fang, C. Cao, Z. Liu, J. Ren and X. Qu, *ACS Nano*, 2019, **13**, 9206-9217.
38. L. Yuan, M. Tian, J. Lan, X. Cao, X. Wang, Z. Chai, J. K. Gibson and W. Shi, *Chem. Comm.*, 2018, **54**, 370-373.
39. Y. Feng, Q. Chen, M. Jiang and J. Yao, *Ind. Eng. Chem. Res.*, 2019, **58**, 17646-17659.
40. S. Chong, G. Thiele and J. Kim, *Nat. Commun.*, 2017, **8**, 1539.
41. X. Chen, Y. Lyu, Z. Wang, X. Qiao, B. C. Gates and D. Yang, *ACS Catal.*, 2020, **10**, 2906-2914.
42. S. Yuan, L. Zou, J. S. Qin, J. Li, L. Huang, L. Feng, X. Wang, M. Bosch, A. Alsalme, T. Cagin and H. C. Zhou, *Nat. Commun.*, 2017, **8**, 15356.
43. D. Yang and B. C. Gates, *ACS Catal.*, 2019, **9**, 1779-1798.
44. S. M. Moosavi, A. Nandy, K. M. Jablonka, D. Ongari, J. P. Janet, P. G. Boyd, Y. Lee, B. Smit and H. J. Kulik, *Nat. Commun.*, 2020, **11**, 4068.
45. E. Haldoupis, S. Nair and D. S. Sholl, *J. Am. Chem. Soc.*, 2010, **132**, 7528-7539.
46. Y. G. Chung, E. Haldoupis, B. J. Bucior, M. Haranczyk, S. Lee, H. Zhang, K. D. Vogiatzis, M. Milisavljevic, S. Ling, J. S. Camp, B. Slater, J. I. Siepmann, D. S. Sholl and R. Q. Snurr, *J. Chem. Eng. Data*, 2019, **64**, 5985-5998.
47. J. Liu, T. A. Goetjen, Q. Wang, J. G. Knapp, M. C. Wasson, Y. Yang, Z. H. Syed, M. Delferro, J. M. Notestein, O. K. Farha and J. T. Hupp, *Chem. Soc. Rev.*, 2022, **51**, 1045-1097.
48. M. J. Kalmutzki, N. Hanikel and O. M. Yaghi, *Sci. Adv.*, 2018, **4**, eaat9180.
49. A. J. Howarth, Y. Liu, P. Li, Z. Li, T. C. Wang, J. T. Hupp and O. K. Farha, *Nat. Rev. Mater.*, 2016, **1**, 1-15.
50. J. E. Mondloch, M. J. Katz, N. Planas, D. Semrouni, L. Gagliardi, J. T. Hupp and O. K. Farha, *Chem. Comm.*, 2014, **50**, 8944-8946.
51. J. Liu, Z. Lu, Z. Chen, M. Rimoldi, A. J. Howarth, H. Chen, S. Alayoglu, R. Q. Snurr, O. K. Farha and J. T. Hupp, *ACS Appl. Mater. Interfaces*, 2021, **13**, 20081-20093.
52. B. Wang, X. L. Lv, D. Feng, L. H. Xie, J. Zhang, M. Li, Y. Xie, J. R. Li and H. C. Zhou, *J. Am. Chem. Soc.*, 2016, **138**, 6204-6216.
53. S. S. Chui, S. M. Lo, J. P. Charmant, A. G. Orpen and I. D. Williams, *Science*, 1999, **283**, 1148-1150.
54. G. Ferey, C. Mellot-Draznieks, C. Serre, F. Millange, J. Dutour, S. Surble and I. Margiolaki, *Science*, 2005, **309**, 2040-2042.
55. L. Oar-Arteta, T. Wezendonk, X. Sun, F. Kapteijn and J. Gascon, *Mater. Chem. Front.*, 2017, **1**, 1709-1745.
56. M. X. Zhao, N. Yang, Z. X. Li and H. S. Xie, *ChemistrySelect*, 2020, **5**, 13681-13689.
57. C. Singh, S. Mukhopadhyay and I. Hod, *Nano Converg.*, 2021, **8**, 1.
58. Z. Li, A. W. Peters, A. E. Platero-Prats, J. Liu, C. W. Kung, H. Noh, M. R. DeStefano, N. M. Schweitzer, K. W. Chapman, J. T. Hupp and O. K. Farha, *J. Am. Chem. Soc.*, 2017, **139**, 15251-15258.
59. H. G. T. Nguyen, N. M. Schweitzer, C.-Y. Chang, T. L. Drake, M. C. So, P. C. Stair, O. K. Farha, J. T. Hupp and S. T. Nguyen, *ACS Catal.*, 2014, **4**, 2496-2500.
60. Y. Ma, X. Han, S. Xu, Z. Wang, W. Li, I. da Silva, S. Chansai, D. Lee, Y. Zou, M. Nikiel, P. Manuel, A. M. Sheveleva, F. Tuna, E. J. L. McInnes, Y. Cheng, S. Rudic, A. J. Ramirez-Cuesta, S. J. Haigh, C. Hardacre, M. Schroder and S. Yang, *J. Am. Chem. Soc.*, 2021, **143**, 10977-10985.
61. A. M. Abdel-Mageed, B. Rungtaweevoranit, M. Parlinska-Wojtan, X. Pei, O. M. Yaghi and R. J. Behm, *J. Am. Chem. Soc.*, 2019, **141**, 5201-5210.
62. X. He, B. G. Looker, K. T. Dinh, A. W. Stubbs, T. Chen, R. J. Meyer, P. Serna, Y. Román-Leshkov, K. M. Lancaster and M. Dincă, *ACS Catal.*, 2020, **10**, 7820-7825.
63. L. Yang, P. Cai, L. Zhang, X. Xu, A. A. Yakovenko, Q. Wang, J. Pang, S. Yuan, X. Zou, N. Huang, Z. Huang and H. C. Zhou, *J. Am. Chem. Soc.*, 2021, **143**, 12129-12137.
64. J. Zhang, B. An, Z. Li, Y. Cao, Y. Dai, W. Wang, L. Zeng, W. Lin and C. Wang, *J. Am. Chem. Soc.*, 2021, **143**, 8829-8837.
65. M. Kømurcu, A. Lazzarini, G. Kaur, E. Borfecchia, S. Øien-Ødegaard, D. Gianolio, S. Bordiga, K. P. Lillerud and U. Olsbye, *Catal. Today*, 2021, **369**, 193-202.
66. Y. Yang, H. Noh, Q. Ma, R. Wang, Z. Chen, N. M. Schweitzer, J. Liu, K. W. Chapman and J. T. Hupp, *ACS Appl. Mater. Interfaces*, 2021, **13**, 36232-36239.
67. X. Wang, X. Zhang, R. Pandharkar, J. Lyu, D. Ray, Y. Yang, S. Kato, J. Liu, M. C. Wasson, T. Islamoglu, Z. Li, J. T. Hupp, C. J. Cramer, L. Gagliardi and O. K. Farha, *ACS Catal.*, 2020, **10**, 8995-9005.
68. M. R. Mian, L. R. Redfern, S. M. Pratik, D. Ray, J. Liu, K. B. Idrees, T. Islamoglu, L. Gagliardi and O. K. Farha, *Chem. Mater.*, 2020, **32**, 3078-3086.
69. C. T. Buru, J. Lyu, J. Liu and O. K. Farha, *Front. Mater. Sci.*, 2019, **6**.
70. Y. Zhang, X. Zhang, J. Lyu, K. I. Otake, X. Wang, L. R. Redfern, C. D. Malliakas, Z. Li, T. Islamoglu, B. Wang and O. K. Farha, *J. Am. Chem. Soc.*, 2018, **140**, 11179-11183.
71. Y. Chen, X. Zhang, M. R. Mian, F. A. Son, K. Zhang, R. Cao, Z. Chen, S. J. Lee, K. B. Idrees, T. A. Goetjen, J. Lyu, P. Li, Q. Xia, Z. Li, J. T. Hupp, T. Islamoglu, A. Napolitano, G. W. Peterson and O. K. Farha, *J. Am. Chem. Soc.*, 2020, **142**, 21428-21438.
72. T. Islamoglu, K.-I. Otake, P. Li, C. T. Buru, A. W. Peters, I. Akpinar, S. J. Garibay and O. K. Farha, *CrystEngComm*, 2018, **20**, 5913-5918.
73. T. He, Y. Z. Zhang, X. J. Kong, J. Yu, X. L. Lv, Y. Wu, Z. J. Guo and J. R. Li, *ACS Appl. Mater. Interfaces*, 2018, **10**, 16650-16659.
74. Y. Zhao, S. Qi, Z. Niu, Y. Peng, C. Shan, G. Verma, L. Wojtas,

Z. Zhang, B. Zhang, Y. Feng, Y. S. Chen and S. Ma, *J. Am. Chem. Soc.*, 2019, **141**, 14443-14450.

75. A. W. Peters, K. Otake, A. E. Platero-Prats, Z. Li, M. R. DeStefano, K. W. Chapman, O. K. Farha and J. T. Hupp, *ACS Appl. Mater. Interfaces*, 2018, **10**, 15073-15078.
76. J. Pang, Z. Di, J. S. Qin, S. Yuan, C. T. Lollar, J. Li, P. Zhang, M. Wu, D. Yuan, M. Hong and H. C. Zhou, *J. Am. Chem. Soc.*, 2020, **142**, 15020-15026.
77. D. Yang, M. A. Ortuno, V. Bernales, C. J. Cramer, L. Gagliardi and B. C. Gates, *J. Am. Chem. Soc.*, 2018, **140**, 3751-3759.
78. G. W. Peterson, G. W. Wagner, A. Balboa, J. Mahle, T. Sewell and C. J. Karwacki, *J. Phys. Chem. C*, 2009, **113**, 13906-13917.
79. A. J. Rieth and M. Dinca, *J. Am. Chem. Soc.*, 2018, **140**, 3461-3466.
80. J. Jiang, F. Gandara, Y. B. Zhang, K. Na, O. M. Yaghi and W. G. Klemperer, *J. Am. Chem. Soc.*, 2014, **136**, 12844-12847.
81. C. A. Trickett, T. M. Osborn Popp, J. Su, C. Yan, J. Weisberg, A. Huq, P. Urban, J. Jiang, M. J. Kalmutzki, Q. Liu, J. Baek, M. P. Head-Gordon, G. A. Somorjai, J. A. Reimer and O. M. Yaghi, *Nat. Chem.*, 2019, **11**, 170-176.
82. A. J. Howarth, T. C. Wang, S. S. Al-Juaid, S. G. Aziz, J. T. Hupp and O. K. Farha, *Dalton Trans.*, 2016, **45**, 93-97.
83. D. Yang, M. Babucci, W. H. Casey and B. C. Gates, *ACS Cent. Sci.*, 2020, **6**, 1523-1533.
84. N. C. Burtch, I. M. Walton, J. T. Hungerford, C. R. Morelock, Y. Jiao, J. Heinen, Y. S. Chen, A. A. Yakovenko, W. Xu, D. Dubbeldam and K. S. Walton, *Nat. Chem.*, 2020, **12**, 186-192.
85. J. Liu, J. Ye, Z. Li, K. I. Otake, Y. Liao, A. W. Peters, H. Noh, D. G. Truhlar, L. Gagliardi, C. J. Cramer, O. K. Farha and J. T. Hupp, *J. Am. Chem. Soc.*, 2018, **140**, 11174-11178.
86. X. Wang, X. Zhang, P. Li, K. I. Otake, Y. Cui, J. Lyu, M. D. Krzyaniak, Y. Zhang, Z. Li, J. Liu, C. T. Buru, T. Islamoglu, M. R. Wasielewski, Z. Li and O. K. Farha, *J. Am. Chem. Soc.*, 2020, **141**, 8306-8314.
87. T. A. Goetjen, X. Zhang, J. Liu, J. T. Hupp and O. K. Farha, *ACS Sustain. Chem. Eng.*, 2019, **7**, 2553-2557.
88. J. Liu, Z. Li, X. Zhang, K.-i. Otake, L. Zhang, A. W. Peters, M. J. Young, N. M. Bedford, S. P. Letourneau, D. J. Mandia, J. W. Elam, O. K. Farha and J. T. Hupp, *ACS Catal.*, 2019, **9**, 3198-3207.
89. J. Li, X. Han, X. Kang, Y. Chen, S. Xu, G. L. Smith, E. Tillotson, Y. Cheng, L. J. McCormick McPherson, S. J. Teat, S. Rudic, A. J. Ramirez-Cuesta, S. J. Haigh, M. Schroder and S. Yang, *Angew. Chem. Int. Ed.*, 2021, **60**, 15541-15547.
90. H. Wang, Z. Shi, J. Yang, T. Sun, B. Rungtaweevoranit, H. Lyu, Y. B. Zhang and O. M. Yaghi, *Angew. Chem. Int. Ed.*, 2021, **60**, 3417-3421.
91. X. L. Lv, L. Feng, L. H. Xie, T. He, W. Wu, K. Y. Wang, G. Si, B. Wang, J. R. Li and H. C. Zhou, *J. Am. Chem. Soc.*, 2021, **143**, 2784-2791.
92. X. Feng, Y. Song, J. S. Chen, Z. Xu, S. J. Dunn and W. Lin, *J. Am. Chem. Soc.*, 2021, **143**, 1107-1118.
93. J. S. Lee, E. A. Kapustin, X. Pei, S. Llopis, O. M. Yaghi and F. D. Toste, *Chem.*, 2020, **6**, 142-152.
94. Y. Yang, X. Zhang, S. Kanchanakungwankul, Z. Lu, H. Noh, Z. H. Syed, O. K. Farha, D. G. Truhlar and J. T. Hupp, *J. Am. Chem. Soc.*, 2020, **142**, 21169-21177.
95. K.-I. Otake, J. Ye, M. Mandal, T. Islamoglu, C. T. Buru, J. T. Hupp, M. Delferro, D. G. Truhlar, C. J. Cramer and O. K. Farha, *ACS Catal.*, 2019, **9**, 5383-5390.
96. K. I. Otake, Y. Cui, C. T. Buru, Z. Li, J. T. Hupp and O. K. Farha, *J. Am. Chem. Soc.*, 2018, **140**, 8652-8656.
97. M. Mandal, C. J. Cramer, D. G. Truhlar, J. Sauer and L. Gagliardi, *ACS Catal.*, 2020, **10**, 10051-10059.
98. M. Wen, Y. Kuwahara, K. Mori, D. Zhang, H. Li and H. Yamashita, *J. Mater. Chem. A*, 2015, **3**, 14134-14141.
99. P. Ji, K. Manna, Z. Lin, X. Feng, A. Urban, Y. Song and W. Lin, *J. Am. Chem. Soc.*, 2017, **139**, 7004-7011.
100. P. Piszczek, A. Radtke, A. Wojtczak, T. Muzioł and J. Chojnacki, *Polyhedron*, 2009, **28**, 279-285.
101. J. G. Park, B. A. Collins, L. E. Darago, T. Runcevski, M. E. Ziebel, M. L. Aubrey, H. Z. H. Jiang, E. Velasquez, M. A. Green, J. D. Goodpaster and J. R. Long, *Nat. Chem.*, 2021, **13**, 594-598.
102. A. J. Rieth, Y. Tulchinsky and M. Dinca, *J. Am. Chem. Soc.*, 2016, **138**, 9401-9404.
103. J. H. Dou, M. Q. Arguilla, Y. Luo, J. Li, W. Zhang, L. Sun, J. L. Mancuso, L. Yang, T. Chen, L. R. Parent, G. Skorupskii, N. J. Libretto, C. Sun, M. C. Yang, P. V. Dip, E. J. Brignole, J. T. Miller, J. Kong, C. H. Hendon, J. Sun and M. Dinca, *Nat. Mater.*, 2021, **20**, 222-228.
104. Z. Li, N. M. Schweitzer, A. B. League, V. Bernales, A. W. Peters, A. B. Getsoian, T. C. Wang, J. T. Miller, A. Vjunov, J. L. Fulton, J. A. Lercher, C. J. Cramer, L. Gagliardi, J. T. Hupp and O. K. Farha, *J. Am. Chem. Soc.*, 2016, **138**, 1977-1982.
105. I. S. Kim, Z. Li, J. Zheng, A. E. Platero-Prats, A. Mavrandonakis, S. Pellizzeri, M. Ferrandon, A. Vjunov, L. C. Gallington, T. E. Webber, N. A. Vermeulen, R. L. Penn, R. B. Getman, C. J. Cramer, K. W. Chapman, D. M. Camaioni, J. L. Fulton, J. A. Lercher, O. K. Farha, J. T. Hupp and A. B. F. Martinson, *Angew. Chem. Int. Ed.*, 2018, **57**, 909-913.
106. C. Marsh, X. Han, J. Li, Z. Lu, S. P. Argent, I. da Silva, Y. Cheng, L. L. Daemen, A. J. Ramirez-Cuesta, S. P. Thompson, A. J. Blake, S. Yang and M. Schroder, *J. Am. Chem. Soc.*, 2021, **143**, 6586-6592.
107. Q. Wang, Z. Pengmei, R. Pandharkar, L. Gagliardi, J. T. Hupp, J. M. Notestein, *J. Catal.*, 2022, **407**, 162-173.
108. A. Bavykina, N. Kolobov, I. S. Khan, J. A. Bau, A. Ramirez and J. Gascon, *Chem. Rev.*, 2020, **120**, 8468-8535.
109. X. Zhang, N. A. Vermeulen, Z. Huang, Y. Cui, J. Liu, M. D. Krzyaniak, Z. Li, H. Noh, M. R. Wasielewski, M. Delferro and O. K. Farha, *ACS Appl. Mater. Interfaces*, 2018, **10**, 635-641.
110. Y. S. Wei, M. Zhang, R. Zou and Q. Xu, *Chem. Rev.*, 2020, **120**, 12089-12174.
111. F. A. Paz, J. Klinowski, S. M. Vilela, J. P. Tome, J. A. Cavaleiro and J. Rocha, *Chem. Soc. Rev.*, 2012, **41**, 1088-1110.

112. Y. Zhang, X. Yang and H.-C. Zhou, *Polyhedron*, 2018, **154**, 189-201.
113. A. H. Vahabi, F. Norouzi, E. Sheibani and M. Rahimi-Nasrabadi, *Coord. Chem. Rev.*, 2021, **445**.
114. B. J. Bucior, A. S. Rosen, M. Haranczyk, Z. Yao, M. E. Ziebel, O. K. Farha, J. T. Hupp, J. I. Siepmann, A. Aspuru-Guzik and R. Q. Snurr, *Cryst. Growth Des.*, 2019, **19**, 6682-6697.
115. M. H. Mahyuddin, Y. Shiota and K. Yoshizawa, *Catal. Sci. Technol.*, 2019, **9**, 1744-1768.
116. J. C. Fornaciari, D. Primc, K. Kawashima, B. R. Wygant, S. Verma, L. Spanu, C. B. Mullins, A. T. Bell and A. Z. Weber, *ACS Energy Lett.*, 2020, **5**, 2954-2963.
117. B. L. Farrell, V. O. Igenegbai and S. Linic, *ACS Catal.*, 2016, **6**, 4340-4346.
118. S. Standl, F. M. Kirchberger, T. Kühlewind, M. Tonigold, M. Sanchez-Sanchez, J. A. Lercher and O. Hinrichsen, *Chem. Eng. J.*, 2020, **402**.
119. P. Tian, Y. Wei, M. Ye and Z. Liu, *ACS Catal.*, 2015, **5**, 1922-1938.
120. S. Ilias and A. Bhan, *ACS Catal.*, 2012, **3**, 18-31.
121. J. Zhong, J. Han, Y. Wei and Z. Liu, *J. Catal.*, 2021, **396**, 23-31.
122. X. Wu, S. Xu, Y. Wei, W. Zhang, J. Huang, S. Xu, Y. He, S. Lin, T. Sun and Z. Liu, *ACS Catal.*, 2018, **8**, 7356-7361.
123. S. Ahn, S. L. Nauert, C. T. Buru, M. Rimoldi, H. Choi, N. M. Schweitzer, J. T. Hupp, O. K. Farha and J. M. Notestein, *J. Am. Chem. Soc.*, 2018, **140**, 8535-8543.
124. B. Bohigues, S. Rojas-Buzo, M. Moliner and A. Corma, *ACS Sustain. Chem. Eng.*, 2021, **9**, 15793-15806.
125. Y. Fan, E. You, Z. Xu and W. Lin, *J. Am. Chem. Soc.*, 2021, **143**, 18871-18876.
126. D. Yang and B. C. Gates, *Acc. Chem. Res.*, 2021, **54**, 1982-1991.
127. D. Yang, C. A. Gaggioli, D. Ray, M. Babucci, L. Gagliardi and B. C. Gates, *J. Am. Chem. Soc.*, 2020, **142**, 8044-8056.
128. Z. Wang, M. Babucci, Y. Zhang, Y. Wen, L. Peng, B. Yang, B. C. Gates and D. Yang, *ACS Appl. Mater. Interfaces*, 2020, **12**, 53537-53546.
129. D. Yang, V. Bernales, T. Islamoglu, O. K. Farha, J. T. Hupp, C. J. Cramer, L. Gagliardi and B. C. Gates, *J. Am. Chem. Soc.*, 2016, **138**, 15189-15196.
130. T. Loiseau, C. Serre, C. Huguenard, G. Fink, F. Taulelle, M. Henry, T. Bataille and G. Ferey, *Chem-Eur. J.*, 2004, **10**, 1373-1382.
131. Q. Yang, S. Vaesen, M. Vishnuvarthan, F. Ragon, C. Serre, A. Vimont, M. Daturi, G. De Weireld and G. Maurin, *J. Mater. Chem.*, 2012, **22**.
132. M. Ermer, J. Mehler, M. Kriesten, Y. S. Avadhut, P. S. Schulz and M. Hartmann, *Dalton Trans.*, 2018, **47**, 14426-14430.
133. M. Rimoldi, V. Bernales, J. Borycz, A. Vjunov, L. C. Gallington, A. E. Platero-Prats, I. S. Kim, J. L. Fulton, A. B. F. Martinson, J. A. Lercher, K. W. Chapman, C. J. Cramer, L. Gagliardi, J. T. Hupp and O. K. Farha, *Chem. Mater.*, 2017, **29**, 1058-1068.
134. M. Ravi, M. Ranocchiari and J. A. van Bokhoven, *Angew. Chem. Int. Ed.*, 2017, **56**, 16464-16483.
135. G. A. Olah, *Angew. Chem. Int. Ed.*, 2005, **44**, 2636-2639.
136. B. V. Kramar, B. T. Phelan, E. A. Sprague-Klein, B. T. Diroll, S. Lee, K.-i. Otake, R. Palmer, M. W. Mara, O. K. Farha, J. T. Hupp and L. X. Chen, *Energy Fuels*, 2021, **35**, 19081-19095.
137. B. E. R. Snyder, M. L. Bols, R. A. Schoonheydt, B. F. Sels and E. I. Solomon, *Chem. Rev.*, 2018, **118**, 2718-2768.
138. A. C. Rosenzweig, C. A. Frederick, S. J. Lippard and P. Nordlund, *Nature*, 1993, **366**, 537-543.
139. R. L. Lieberman and A. C. Rosenzweig, *Nature*, 2005, **434**, 177-182.
140. A. S. Hakemian and A. C. Rosenzweig, *Annu. Rev. Biochem.*, 2007, **76**, 223-241.
141. V. C. Wang, S. Maji, P. P. Chen, H. K. Lee, S. S. Yu and S. I. Chan, *Chem. Rev.*, 2017, **117**, 8574-8621.
142. M. O. Ross, F. MacMillan, J. Wang, A. Nisthal, T. J. Lawton, B. D. Olafson, S. L. Mayo, A. C. Rosenzweig and B. M. Hoffman, *Science*, 2019, **364**, 566-570.
143. K. Narsimhan, K. Iyoki, K. Dinh and Y. Roman-Leshkov, *ACS Cent. Sci.*, 2016, **2**, 424-429.
144. V. L. Sushkevich and J. A. van Bokhoven, *ACS Catal.*, 2019, **9**, 6293-6304.
145. J. Ohyama, A. Hirayama, Y. Tsuchimura, N. Kondou, H. Yoshida, M. Machida, S. Nishimura, K. Kato, I. Miyazato and K. Takahashi, *Catal. Sci. Technol.*, 2021, **11**, 3437-3446.
146. J. Zheng, J. Ye, M. A. Ortuno, J. L. Fulton, O. Y. Gutierrez, D. M. Camaioni, R. K. Motkuri, Z. Li, T. E. Webber, B. L. Mehdi, N. D. Browning, R. L. Penn, O. K. Farha, J. T. Hupp, D. G. Truhlar, C. J. Cramer and J. A. Lercher, *J. Am. Chem. Soc.*, 2019, **141**, 9292-9304.
147. T. Ikuno, J. Zheng, A. Vjunov, M. Sanchez-Sanchez, M. A. Ortuno, D. R. Pahls, J. L. Fulton, D. M. Camaioni, Z. Li, D. Ray, B. L. Mehdi, N. D. Browning, O. K. Farha, J. T. Hupp, C. J. Cramer, L. Gagliardi and J. A. Lercher, *J. Am. Chem. Soc.*, 2017, **139**, 10294-10301.
148. H. A. Doan, Z. Li, O. K. Farha, J. T. Hupp and R. Q. Snurr, *Catal. Today*, 2018, **312**, 2-9.
149. X. Zhu, Q. Imtiaz, F. Donat, C. R. Müller and F. Li, *Energy Environ. Sci.*, 2020, **13**, 772-804.
150. H. B. Gray and J. R. Winkler, *Acc. Chem. Res.*, 2018, **51**, 1850-1857.
151. V. A. Larson, B. Battistella, K. Ray, N. Lehnert and W. Nam, *Nat. Rev. Chem.*, 2020, **4**, 404-419.
152. M. Ren, Q. Shi, L. Mi, W. Liang, M. Yuan, L. Wang, Z. Gao, W. Huang, J. Huang and Z. Zuo, *Mater. Today Sustain.*, 2021, **11-12**.
153. D. Y. Osadchii, A. I. Olivos-Suarez, Á. Szécsényi, G. Li, M. A. Nasalevich, I. A. Dugulan, P. S. Crespo, E. J. M. Hensen, S. L. Veber, M. V. Fedin, G. Sankar, E. A. Pidko and J. Gascon, *ACS Catal.*, 2018, **8**, 5542-5548.
154. A. Szecsenyi, G. Li, J. Gascon and E. A. Pidko, *Chem. Sci.*, 2018, **9**, 6765-6773.

155. J. Baek, B. Rungtaweevoranit, X. Pei, M. Park, S. C. Fakra, Y. S. Liu, R. Matheu, S. A. Alshmimri, S. Alshehri, C. A. Trickett, G. A. Somorjai and O. M. Yaghi, *J. Am. Chem. Soc.*, 2018, **140**, 18208-18216.
156. L. Cao, O. Caldararu, A. C. Rosenzweig and U. Ryde, *Angew. Chem. Int. Ed.*, 2018, **57**, 162-166.
157. Y. J. Colon and R. Q. Snurr, *Chem. Soc. Rev.*, 2014, **43**, 5735-5749.
158. D. Chen, W. Yang, L. Jiao, L. Li, S. H. Yu and H. L. Jiang, *Adv. Mater.*, 2020, **32**, e2000041.
159. A. S. Rosen, J. M. Notestein and R. Q. Snurr, *J. Comput. Chem.*, 2019, **40**, 1305-1318.
160. P. Liao, R. B. Getman and R. Q. Snurr, *ACS Appl. Mater. Interfaces*, 2017, **9**, 33484-33492.
161. L. J. Wang, H. Deng, H. Furukawa, F. Gandara, K. E. Cordova, D. Peri and O. M. Yaghi, *Inorg. Chem.*, 2014, **53**, 5881-5883.
162. M. Märcz, R. E. Johnsen, P. D. C. Dietzel and H. Fjellvåg, *Microporous Mesoporous Mater.*, 2012, **157**, 62-74.
163. W. L. Queen, E. D. Bloch, C. M. Brown, M. R. Hudson, J. A. Mason, L. J. Murray, A. J. Ramirez-Cuesta, V. K. Peterson and J. R. Long, *Dalton Trans.*, 2012, **41**, 4180-4187.
164. A. S. Rosen, J. M. Notestein and R. Q. Snurr, *ACS Catal.*, 2019, **9**, 3576-3587.
165. M. Barona and R. Q. Snurr, *ACS Appl. Mater. Interfaces*, 2020, **12**, 28217-28231.
166. J. G. Vitillo, A. Bhan, C. J. Cramer, C. C. Lu and L. Gagliardi, *ACS Catal.*, 2019, **9**, 2870-2879.
167. J. G. Vitillo, C. C. Lu, C. J. Cramer, A. Bhan and L. Gagliardi, *ACS Catal.*, 2020, **11**, 579-589.
168. A. S. Rosen, J. M. Notestein and R. Q. Snurr, *Angew. Chem. Int. Ed.*, 2020, **59**, 19494-19502.
169. P. Kalck, C. L. Berre, P. Serp, *Coord. Chem. Rev.*, 2020, **402**, 213078.
170. M. V. Kirillova, M. L. Kuznetsov, P. M. Reis, J. A. da Silva, J. J. da Silva and A. J. Pombeiro, *J. Am. Chem. Soc.*, 2007, **129**, 10531-10545.
171. Y. Taniguchi, T. Hayashida, H. Shibasaki, D. G. Piao, T. Kitamura, T. Yamaji and Y. Fujiwara, *Org. Lett.*, 1999, **1**, 557-559.
172. A. Phan, A. U. Czaja, F. Gandara, C. B. Knobler and O. M. Yaghi, *Inorg. Chem.*, 2011, **50**, 7388-7390.
173. T. A. Goetjen, J. Liu, Y. Wu, J. Sui, X. Zhang, J. T. Hupp and O. K. Farha, *Chem. Comm.*, 2020, **56**, 10409-10418.
174. S. Jakobsen, D. Gianolio, D. S. Wragg, M. H. Nilsen, H. Emerich, S. Bordiga, C. Lamberti, U. Olsbye, M. Tilset and K. P. Lillerud, *Phys. Rev. B*, 2012, **86**.
175. A. A. Fonseca, R. H. Heyn, M. Frøseth, J. W. Thybaut, J. Poissonnier, A. Meiswinkel, H.-J. Zander and J. Canivet, *Johnson Matthey Technol. Rev.*, 2021, **65**, 311-329.
176. J. F. Hartwig, *Acc. Chem. Res.*, 2012, **45**, 864-873.
177. C. N. Iverson and M. R. Smith, *J. Am. Chem. Soc.*, 1999, **121**, 7696-7697.
178. J. Y. Cho, C. N. Iverson and M. R. Smith, *J. Am. Chem. Soc.*, 2000, **122**, 12868-12869.
179. J. Y. Cho, M. K. Tse, D. Holmes, R. E. Maleczka, Jr. and M. R. Smith, 3rd, *Science*, 2002, **295**, 305-308.
180. A. K. Cook, S. D. Schimler, A. J. Matzger and M. S. Sanford, *Science*, 2016, **351**, 1421-1424.
181. K. T. Smith, S. Berritt, M. Gonzalez-Moreiras, S. Ahn, M. R. Smith, 3rd, M. H. Baik and D. J. Mindiola, *Science*, 2016, **351**, 1424-1427.
182. X. Zhang, Z. Huang, M. Ferrandon, D. Yang, L. Robison, P. Li, T. C. Wang, M. Delferro and O. K. Farha, *Nat. Catal.*, 2018, **1**, 356-362.
183. Z. H. Syed, Z. Chen, K. B. Idrees, T. A. Goetjen, E. C. Wegener, X. Zhang, K. W. Chapman, D. M. Kaphan, M. Delferro and O. K. Farha, *Organometallics*, 2020, **39**, 1123-1133.
184. B. Yang, X.-P. Wu, L. Gagliardi and D. G. Truhlar, *Theor. Chem. Acc.*, 2019, **138**.
185. X. Feng, Y. Song, Z. Li, M. Kaufmann, Y. Pi, J. S. Chen, Z. Xu, Z. Li, C. Wang and W. Lin, *J. Am. Chem. Soc.*, 2019, **141**, 11196-11203.
186. D. J. Xiao, E. D. Bloch, J. A. Mason, W. L. Queen, M. R. Hudson, N. Planas, J. Borycz, A. L. Dzubak, P. Verma, K. Lee, F. Bonino, V. Crocella, J. Yano, S. Bordiga, D. G. Truhlar, L. Gagliardi, C. M. Brown and J. R. Long, *Nat. Chem.*, 2014, **6**, 590-595.
187. P. Verma, K. D. Vogiatzis, N. Planas, J. Borycz, D. J. Xiao, J. R. Long, L. Gagliardi and D. G. Truhlar, *J. Am. Chem. Soc.*, 2015, **137**, 5770-5781.
188. A. Kazaryan and E. J. Baerends, *ACS Catal.*, 2015, **5**, 1475-1488.
189. B. L. Suh and J. Kim, *J. Phys. Chem. C*, 2018, **122**, 23078-23083.
190. M. C. Simons, J. G. Vitillo, M. Babucci, A. S. Hoffman, A. Boubnov, M. L. Beauvais, Z. Chen, C. J. Cramer, K. W. Chapman, S. R. Bare, B. C. Gates, C. C. Lu, L. Gagliardi and A. Bhan, *J. Am. Chem. Soc.*, 2019, **141**, 18142-18151.
191. Z. Li, A. W. Peters, V. Bernales, M. A. Ortuno, N. M. Schweitzer, M. R. DeStefano, L. C. Gallington, A. E. Platero-Prats, K. W. Chapman, C. J. Cramer, L. Gagliardi, J. T. Hupp and O. K. Farha, *ACS Cent. Sci.*, 2017, **3**, 31-38.
192. M. C. Simons, M. A. Ortuño, V. Bernales, C. A. Gaggioli, C. J. Cramer, A. Bhan and L. Gagliardi, *ACS Catal.*, 2018, **8**, 2864-2869.
193. M. Barona, S. Ahn, W. Morris, W. Hoover, J. M. Notestein, O. K. Farha and R. Q. Snurr, *ACS Catal.*, 2019, **10**, 1460-1469.
194. Y. Zhang, L. Qi, B. Leonhardt, and A. T. Bell, *ACS Catal.* 2022, **12**, 3333-3345.
195. J. W. Lee, H. Lee, U. G. Hong, J. Lee, Y. Cho, Y. Yoo, H. Jang, I. K. Song, *J. Ind. Eng. Chem.* 2012, **18**, 1096-1101.
196. M. Bergaoui, M. Khalfaoui, A. Awadallah-F and S. Al-Muhtaseb, *J. Nat. Gas Sci. Eng.*, 2021, **96**.
197. P. Liu, E. Redekop, X. Gao, W. C. Liu, U. Olsbye and G. A. Somorjai, *J. Am. Chem. Soc.*, 2019, **141**, 11557-11564.

198. D. A. Gomez-Gualdron, S. T. Dix, R. B. Getman and R. Q. Snurr, *Phys. Chem. Chem. Phys.*, 2015, **17**, 27596-27608.
199. S. T. Dix, D. A. Gómez-Gualdrón and R. B. Getman, *Surf. Sci.*, 2016, **653**, 11-21.
200. J. Zhu and R. B. Getman, *Ind. Eng. Chem. Res.*, 2018, **57**, 5580-5590.
201. B. Schweitzer, C. Archuleta, B. Seong, R. Anderson and D. A. Gomez-Gualdron, *Phys. Chem. Chem. Phys.*, 2020, **22**, 2475-2487.
202. C. J. Stephenson, J. T. Hupp and O. K. Farha, *Inorg. Chem. Front.*, 2015, **2**, 448-452.
203. S. T. Dix, J. K. Scott, R. B. Getman, C. T. Campbell, *Faraday Discuss.*, 2016, **188**, 21-38.
204. C. L. Hobday, C. H. Woodall, M. J. Lennox, M. Frost, K. Kamenev, T. Duren, C. A. Morrison, S. A. Moggach, *Nat. Commun.*, 2018, **9**, 1429.
205. D. Fairen-Jimenez, R. Galvelis, A. Torrisi, A. D. Gellan, M. T. Wharmby, P. A. Wright, C. Mellot-Draznieks, T. Duren, *Dalton. Trans.* 2012, **41**, 10752–10762.
206. C. Zhang, J. A. Gee, D. S. Sholl, R. P. Lively, *J. Phys. Chem. C.* 2014, **118**, 20727–20733.
207. T. Tian, M. T. Wharmby, J. B. Parra, C. O. Ania, D. Fairen-Jimenez, *Dalton. Trans.*, 2016, **45**, 6893–6900.
208. A. E. Platero-Prats, A. Mavrandonakis, J. Liu, Z. Chen, Z. Chen, Z. Li, A. A. Yakovenko, L. C. Gallington, J. T. Hupp, O. K. Farha, C. J. Cramer and K. W. Chapman, *J. Am. Chem. Soc.*, 2021, **143**, 20090-20094.
209. M. R. Bray, R. J. Deeth, *Inorg. Chem.* 1996, **35**, 5720-5724.
210. W. Feduska and A. O. Isenberg, *J. Power Sources*, 1983, **10**, 89-102.
211. D. J. Brett, A. Atkinson, N. P. Brandon and S. J. Skinner, *Chem. Soc. Rev.*, 2008, **37**, 1568-1578.
212. M. Fallah Vostakola and B. Amini Horri, *Energies*, 2021, **14**.
213. C. W. Kung, S. Goswami, I. Hod, T. C. Wang, J. Duan, O. K. Farha and J. T. Hupp, *Acc. Chem. Res.*, 2020, **53**, 1187-1195.
214. S. Najari, S. Saeidi, P. Concepcion, D. D. Dionysiou, S. K. Bhargava, A. F. Lee and K. Wilson, *Chem. Soc. Rev.*, 2021, **50**, 4564-4605.
215. Q. Wang and D. Astruc, *Chem. Rev.*, 2020, **120**, 1438-1511.
216. H. Konnerth, B. M. Matsagar, S. S. Chen, M. H. G. Prechtl, F.-K. Shieh and K. C. W. Wu, *Coord. Chem. Rev.*, 2020, **416**, 213319.